L^2 Stable Discontinuous Galerkin Methods for One-dimensional Two-way Wave Equations

Yingda Cheng,* Ching-Shan Chou,† Fengyan Li,‡ and Yulong Xing§

July 15, 2015

Abstract

Simulating wave propagation is one of the fundamental problems in scientific computing. In this paper, we consider one-dimensional two-way wave equations, and investigate a family of L^2 stable high order discontinuous Galerkin methods defined through a general form of numerical fluxes. For these L^2 stable methods, we systematically establish stability (hence energy conservation), error estimates (in both L^2 and negative-order norms), and dispersion analysis. One novelty of this work is to identify a sub-family of the numerical fluxes, termed $\alpha\beta$-fluxes. Discontinuous Galerkin methods with $\alpha\beta$-fluxes are proven to have optimal L^2 error estimates and superconvergence properties. Moreover, both the upwind and alternating fluxes belong to this sub-family. Dispersion analysis, which examines both the physical and spurious modes, provides insights into the sub-optimal accuracy of the methods using the central flux and the odd degree polynomials, and demonstrates the importance of numerical initialization for the proposed non-dissipative schemes. Numerical examples are presented to illustrate the accuracy and the long-term behavior of the methods under consideration.

1   Introduction

Wave propagation is a fundamental form of energy transmission, which arises in many fields of science, engineering and industry, and it is significant to geoscience, petroleum engineering and electromagnetics. A vast amount of research has been done for wave simulations, and the commonly used numerical methods range from finite difference, finite volume to spectral element and finite element methods ([18, 17, 24, 15] and references therein, [35, 4, 30]). Among various numerical methods, each with their own advantages, here we will confine our attention to discontinuous Galerkin (DG) methods. DG methods belong to a class of finite element methods using piecewise polynomial spaces for both the numerical solution and the test function. They were originally devised to solve hyperbolic conservation laws, e.g. [26, 12, 14]. The methods can be easily designed to have arbitrary order of accuracy. They are flexible with unstructured meshes, and are

1

natural candidates for *h-p* adaptivity. These methods are known to be highly efficient in parallel computation, due to the compact stencils. Importantly, DG methods perform well in long-term wave simulations [21, 1, 8], given their excellent dispersive and dissipative properties.

In this paper, we consider the one-dimensional linear two-way wave problem,

$$E_t = B_x - S_1, \tag{1.1a}$$

$$B_t = E_x - S_2, \tag{1.1b}$$

where $E = E(t,x)$ and $B = B(t,x)$ are unknown functions, and $S_1 = S_1(t,x)$ and $S_2 = S_2(t,x)$ are both source terms. Note that the system (1.1) is equivalent to the second-order wave equation. Moreover, Maxwell's equations can be viewed as a special case when $S_2 = 0$. As a hyperbolic system, (1.1) can be computed by DG methods directly, yet the key properties of the methods lie in the choices of the numerical fluxes. For example, it is known that the use of either an alternating flux or central flux will give an energy preserving scheme, while the use of the upwind flux will result in a decreasing discrete energy. Moreover, the L^2 error bounds with alternating and upwind fluxes are optimal, while with central flux, the accuracy may be sub-optimal. This leads to the question that, whether we can find a general principle of selecting numerical fluxes, and furthermore, understand the accuracy, stability, energy conservation, and other properties of the resulted numerical methods.

The goal of this paper is to perform a detailed and systematic investigation for a general family of L^2 stable DG methods. Note that the L^2 norm of (E, B) for system (1.1) is equivalent to the total energy, which many DG methods attempt to capture [16, 20, 10, 32, 9]. The proposed methods are defined through a group of numerical fluxes which are certain linear combinations of jumps and averages of the numerical solutions at the cell interfaces with three parameters α, β_1, β_2 involved. In a previous work by Ainsworth and colleagues [3], the same family of fluxes were considered with emphasis on dispersion analysis. For these L^2 stable methods, we will establish stability and hence the energy conservation, error estimates in both L^2 and negative-order norms, superconvergence, and dispersion analysis.

One novelty of this work is that, in search of DG methods with optimal L^2 error estimate, we identify a sub-family of the numerical fluxes, termed $\alpha\beta$-fluxes, that are determined by a specific relation among α, β_1, β_2. This relation, which is satisfied by the widely known upwind and alternating fluxes, was introduced in [3] to characterize different modes in dispersion analysis for DG methods solving two-dimensional second-order wave equations. The relation is used in this work to design a new projection operator, a key component in our proof for the optimal error estimates. Besides the optimal L^2 accuracy, we further prove superconvergence properties for the DG methods with $\alpha\beta$-fluxes by following the analysis in [34] for the linear advection equation. Such superconvergence seems to be uniquely enjoyed by DG methods associated with the $\alpha\beta$-fluxes as suggested numerically.

For the proposed general L^2 stable DG methods, we also systematically perform the dispersion analysis, and present the negative-order norm error estimates as well as the related post-processing techniques similar to those in [13, 23]. For long time wave simulations, it is important to understand the dispersive and dissipative properties of the numerical methods. Our dispersion analysis, which takes a different viewpoint from [3], examines both the physical and spurious modes. In particular, it gives insights into the sub-optimal accuracy of DG methods with the central flux and the odd degree polynomials, and demonstrates the importance of numerical initialization for the proposed non-dissipative schemes. Related work on the dispersion analysis of semi-discrete or fully discrete DG methods in literature can be found in [22, 28, 21, 1, 3, 27, 33, 2].

The remaining of this paper is organized as follows. In Section 2, we introduce a general family of L^2 stable DG methods for one-dimensional two-way wave equations, and also define a

sub-family of the methods associated with $\alpha\beta$-fluxes. We provide in Section 2.1 the analysis of L^2 stability and energy conserving property, and this is followed by L^2 error estimates in Section 2.2 for the general L^2 stable DG methods. In Section 2.3, we present the superconvergence results and postprocessing techniques. The dispersion analysis is performed in Section 2.4. Section 3 contains numerical examples to illustrate the performance of the proposed methods, and we conclude with a few remarks in Section 4.

2 L^2 stable DG methods

In this section, we will formulate a general family of semi-discrete DG methods which is L^2 stable for the one-dimensional two-way wave equations (1.1). Here we consider periodic boundary conditions for simplicity. We start with a mesh of the computational domain $\Omega = [a,b]$, $a = x_{\frac{1}{2}} < x_{\frac{3}{2}} < \cdots < x_{N+\frac{1}{2}} = b$. Each cell is denoted as $I_j = [x_{j-\frac{1}{2}}, x_{j+\frac{1}{2}}]$, with its center $x_j = \frac{1}{2}(x_{j-\frac{1}{2}} + x_{j+\frac{1}{2}})$ and the length $h_j = x_{j+\frac{1}{2}} - x_{j-\frac{1}{2}}$. Let $h = \max_{1 \le j \le N} h_j$. The mesh is assumed to be quasi-uniform, namely, there exists a positive constant σ, such that $\frac{h}{\min_j h_j} < \sigma$, as the mesh is refined. We now define a finite dimensional discrete space,

$$V_h^r = \{v : v|_{I_j} \in P^r(I_j),\ j = 1, 2, \cdots, N\}, \tag{2.1}$$

which consists of piecewise polynomials of degree up to r with respect to the mesh. Note that functions in V_h^r are allowed to have discontinuities across element interfaces. For any $v \in V_h^r$, we denote by $v_{j+\frac{1}{2}}^+$ and $v_{j+\frac{1}{2}}^-$ the limit values of v at $x_{j+\frac{1}{2}}$ from the right cell I_{j+1} and from the left cell I_j, respectively. We use the usual notation $[v]_{j+\frac{1}{2}} = v_{j+\frac{1}{2}}^+ - v_{j+\frac{1}{2}}^-$ and $\{v\}_{j+\frac{1}{2}} = \frac{1}{2}(v_{j+\frac{1}{2}}^+ + v_{j+\frac{1}{2}}^-)$ to represent the jump and the average of the function v at $x_{j+\frac{1}{2}}$ for any j.

The semi-discrete DG method for the system (1.1) is formulated as follows: find $E_h(t, \cdot)$, $B_h(t, \cdot) \in V_h^r$, such that

$$\int_{I_j} (E_h)_t \phi\, dx + \int_{I_j} B_h \phi_x\, dx - \big(\mathcal{F}_B(B_h, E_h)\phi^-\big)_{j+\frac{1}{2}} + \big(\mathcal{F}_B(B_h, E_h)\phi^+\big)_{j-\frac{1}{2}} = \int_{I_j} S_1 \phi\, dx, \tag{2.2a}$$

$$\int_{I_j} (B_h)_t \psi\, dx + \int_{I_j} E_h \psi_x\, dx - \big(\mathcal{F}_E(E_h, B_h)\psi^-\big)_{j+\frac{1}{2}} + \big(\mathcal{F}_E(E_h, B_h)\psi^+\big)_{j-\frac{1}{2}} = \int_{I_j} S_2 \psi\, dx, \tag{2.2b}$$

for all test functions ϕ, $\psi \in V_h^r$, and for all j. By summing up the two equations in (2.2) over all mesh elements, we can write the DG method in a more compact form. We look for $E_h(t, \cdot)$, $B_h(t, \cdot) \in V_h^r$, such that

$$a_h(E_h, B_h; \phi, \psi) = \mathcal{S}(\phi, \psi), \qquad \forall \phi, \psi \in V_h^r, \tag{2.3}$$

where

$$a_h(E_h, B_h; \phi, \psi) = \int_\Omega (E_h)_t \phi\, dx + \sum_j \left(\int_{I_j} B_h \phi_x\, dx + (\mathcal{F}_B(B_h, E_h)[\phi])_{j-\frac{1}{2}} \right)$$

$$+ \int_\Omega (B_h)_t \psi\, dx + \sum_j \left(\int_{I_j} E_h \psi_x\, dx + (\mathcal{F}_E(E_h, B_h)[\psi])_{j-\frac{1}{2}} \right), \tag{2.4}$$

and $\mathcal{S}(\phi, \psi) = \int_\Omega S_1 \phi + S_2 \psi\, dx$.

3

Both the terms $\mathcal{F}_B$ and $\mathcal{F}_E$ in (2.2) are numerical fluxes, and they are single-valued functions defined on the cell interfaces and should be designed to ensure numerical stability and accuracy. In the present work, we consider the following numerical fluxes,

$$\mathcal{F}_B(B_h, E_h) = \{B_h\} + \alpha[B_h] + \beta_1[E_h], \tag{2.5a}$$
$$\mathcal{F}_E(E_h, B_h) = \{E_h\} - \alpha[E_h] + \beta_2[B_h]. \tag{2.5b}$$

Here α, β_1, β_2 are constants that are taken to be $O(1)$, with β_1 and β_2 being non-negative. These numerical fluxes were considered in [3], and they are consistent, that is,

$$\mathcal{F}_B(B, E) = B, \qquad \mathcal{F}_E(E, B) = E. \tag{2.6}$$

The DG methods with fluxes (2.5) define a very general family of L^2 stable DG methods for the system (1.1). Note that the numerical fluxes (2.5) include several commonly used ones in literature. For examples, when $\alpha = 0, \beta_1 = \beta_2 = \frac{1}{2}$, we have the upwind flux; when $\alpha = \beta_1 = \beta_2 = 0$, we have the central flux, and the alternating flux is obtained when $\alpha = \pm\frac{1}{2}, \beta_1 = \beta_2 = 0$.

One novelty of this work is that we further identify a sub-family of the numerical fluxes (2.5), named $\alpha\beta$-fluxes, and the corresponding DG methods have some important provable results in terms of L^2 error estimates and superconvergence, which will be carried out in Sections 2.2 and 2.3.

Definition 2.1. *An $\alpha\beta$-flux is a numerical flux (2.5) when α and $\beta_i \geq 0$ ($i = 1, 2$) satisfy*

$$\alpha^2 + \beta_1\beta_2 = \frac{1}{4}. \tag{2.7}$$

When $\beta_1 = \beta_2 = \beta$, an $\alpha\beta$-flux can be determined by a single parameter α. (Here β is non-negative and $\beta = \sqrt{\frac{1}{4} - \alpha^2}$.) It is easy to see that both the upwind and alternating fluxes are special cases of this $\alpha\beta$-flux family.

Remark 2.1. *One can further generalize the numerical flux in (2.5) as follows,*

$$\mathcal{F}_B(B_h, E_h) = \{B_h\} + \alpha_1[B_h] + \beta_1[E_h], \tag{2.8a}$$
$$\mathcal{F}_E(E_h, B_h) = \{E_h\} + \alpha_2[E_h] + \beta_2[B_h], \tag{2.8b}$$

which involves four parameters. In this work, we will only present analysis for the DG methods with (2.5), and will summarize the L^2 stability and error estimates for the more general DG methods with (2.8) in Remark 2.3 and Remark 2.8. The parameters β_1 and β_2 are chosen to be non-negative to ensure that the proposed DG methods are stable (see Theorem 2.2). In addition, there is no benefit in terms of accuracy or stability if we allow α, β_1 and β_2 to be more general than $O(1)$.

2.1 L^2 stability and energy conservation

In this section, we will establish the L^2 stability, which also informs about the energy conservation property, for the semi-discrete DG method with the general numerical flux (2.5). It suffices to consider $S_1 = S_2 = 0$.

Theorem 2.2. *With $S_1 = S_2 = 0$, the semi-discrete DG scheme (2.2) (or (2.3)) with the numerical flux (2.5) and $\beta_i \geq 0$, $i = 1, 2$, satisfies*

$$\frac{d}{dt}\mathcal{E}_h(t) = -\sum_j \left(\beta_1[E_h]^2 + \beta_2[B_h]^2\right)_{j-\frac{1}{2}} \leq 0, \tag{2.9}$$

4

where

$$\mathcal{E}_h(t) = \frac{1}{2} \int_\Omega (E_h(t,x))^2 + (B_h(t,x))^2 dx$$

is the energy of the system (1.1) at time t.

Proof. We first introduce

$$H_j^{(1)}(B_h, E_h; \phi) = -\int_{I_j} B_h \phi_x dx + (\mathcal{F}_B(B_h, E_h)\phi^-)_{j+\frac{1}{2}} - (\mathcal{F}_B(B_h, E_h)\phi^+)_{j-\frac{1}{2}},$$

$$H_j^{(2)}(E_h, B_h; \psi) = -\int_{I_j} E_h \psi_x dx + (\mathcal{F}_E(E_h, B_h)\psi^-)_{j+\frac{1}{2}} - (\mathcal{F}_E(E_h, B_h)\psi^+)_{j-\frac{1}{2}}.$$

With periodic boundary conditions and the specific definition of the general numerical flux in (2.5), as well as the identity $[\phi\psi] = \{\psi\}[\phi] + \{\phi\}[\psi]$, the following holds for any $\phi, \psi \in V_h^r$,

$$\sum_j H_j^{(1)}(\psi, \phi; \phi) + H_j^{(2)}(\phi, \psi; \psi) = \sum_j \left([\phi\psi] - \mathcal{F}_E(\phi, \psi)[\psi] - \mathcal{F}_B(\psi, \phi)[\phi]\right)_{j-\frac{1}{2}}$$

$$= -\sum_j \left(\beta_1[\phi]^2 + \beta_2[\psi]^2\right)_{j-\frac{1}{2}}. \tag{2.10}$$

Using the definition of a_h in (2.4), one further has

$$a_h(\phi, \psi; \phi, \psi) = \int_\Omega (\phi_t \phi + \psi_t \psi) dx - \sum_j \left(H_j^{(1)}(\psi, \phi; \phi) + H_j^{(2)}(\phi, \psi; \psi)\right)$$

$$= \frac{1}{2}\frac{d}{dt}\int_\Omega (\phi^2 + \psi^2) dx + \sum_j \left(\beta_1[\phi]^2 + \beta_2[\psi]^2\right)_{j-\frac{1}{2}}. \tag{2.11}$$

Now in the semi-discrete DG method with $S_1 = S_2 = 0$, we take $\phi = E_h$ in (2.2a) and $\psi = B_h$ in (2.2b), and get $a_h(E_h, B_h; E_h, B_h) = 0$. This, combined with the general result in (2.11), gives the L^2 stability in (2.9). □

Note that all flux choices with $\beta_i \geq 0$, $i = 1, 2$, produce L^2 stable numerical solutions. In particular, the semi-discrete DG method with either the central or alternating, or the more general flux (2.5) with $\beta_1 = \beta_2 = 0$, preserves the energy of the system. On the other hand, with the commonly used upwind flux ($\alpha = 0, \beta_1 = \beta_2 = \frac{1}{2}$), the L^2 energy decays with time, as expected.

Remark 2.3. *For the source free problem, it can be shown that the semi-discrete DG scheme (2.2) (or (2.3)) with the more general numerical flux (2.8) and $\beta_i \geq 0$, $i = 1, 2$, $(\alpha_1 + \alpha_2)^2 \leq 4\beta_1\beta_2$, satisfies*

$$\frac{d}{dt}\mathcal{E}_h(t) = -\sum_j \left(\beta_1[E_h]^2 + \beta_2[B_h]^2 + (\alpha_1 + \alpha_2)[E_h][B_h]\right)_{j-\frac{1}{2}} \leq 0.$$

2.2 L^2 error estimates

In this section, we will establish error estimates in the L^2-norm for the semi-discrete DG schemes up to a given time $T < \infty$ with various choices of numerical fluxes. The following projections, defined from $H^{r+1}(\Omega)$ onto V_h^r, will be used in the analysis.

1. L^2 projection P_h: $P_h w \in V_h^r$, such that $\forall j$

$$\int_{I_j} P_h w \, v \, dx = \int_{I_j} w \, v \, dx, \qquad \forall v \in P^r(I_j). \tag{2.12}$$

2. Gauss-Radau projection P_h^-: $P_h^- w \in V_h^r$, such that $\forall j$

$$\int_{I_j} P_h^- w \, v \, dx = \int_{I_j} w \, v \, dx, \qquad \forall v \in P^{r-1}(I_j), \tag{2.13}$$

and $(P_h^- w)_{j+\frac{1}{2}}^- = w_{j+\frac{1}{2}}^-$.

3. Gauss-Radau projection P_h^+: $P_h^+ w \in V_h^r$, such that $\forall j$

$$\int_{I_j} P_h^+ w \, v \, dx = \int_{I_j} w \, v \, dx, \qquad \forall v \in P^{r-1}(I_j), \tag{2.14}$$

and $(P_h^+ w)_{j-\frac{1}{2}}^+ = w_{j-\frac{1}{2}}^+$.

These projections are commonly used in analyzing DG methods for one-dimensional problems, and the following approximation property can be easily established [11]:

$$\|w - \pi_h w\|^2 + h \sum_j ((w - \pi_h w)_{j+\frac{1}{2}}^\pm)^2 \leq C_\star h^{2r+2} \|w\|_{H^{r+1}}^2. \tag{2.15}$$

Here $\pi_h = P_h, P_h^-$ or P_h^+, and $w - \pi_h w$ gives the projection error associated with the projection π_h. In (2.15), $\|\cdot\|$ and $\|\cdot\|_{H^{r+1}}$ stand for the L^2-norm and H^{r+1}-norm in Ω, respectively. The constant $C_\star$ depends on r but not on h or w. Throughout the paper, $C_\star$ will be used to denote a generic constant which may depend on r and mesh parameter σ. We also use C to denote another generic constant, independent of h, but it may depend on r, mesh parameter σ, and some Sobolev norms of the exact solution of (1.1) up to time T. Both C and $C_\star$ may take different values at different occurrences. In the analysis, the following inverse equality will also be needed [11],

$$h^2 \int_{I_j} (v_x)^2 dx + h \left((v_{j-\frac{1}{2}}^+)^2 + (v_{j+\frac{1}{2}}^-)^2 \right) \leq C_\star \int_{I_j} v^2 dx, \qquad \forall v \in V_h^r. \tag{2.16}$$

Now we define the numerical error e_h of the semi-discrete DG method,

$$e_h = \begin{pmatrix} e_B \\ e_E \end{pmatrix} := \begin{pmatrix} B \\ E \end{pmatrix} - \begin{pmatrix} B_h \\ E_h \end{pmatrix}.$$

This error function can be further decomposed into two parts, $e_h = \eta_h + \zeta_h$, where

$$\eta_h = \begin{pmatrix} \eta_B \\ \eta_E \end{pmatrix} := \begin{pmatrix} B \\ E \end{pmatrix} - \pi_h \begin{pmatrix} B \\ E \end{pmatrix}, \qquad \zeta_h = \begin{pmatrix} \zeta_B \\ \zeta_E \end{pmatrix} := \pi_h \begin{pmatrix} B \\ E \end{pmatrix} - \begin{pmatrix} B_h \\ E_h \end{pmatrix}.$$

Here π_h is some linear operator from $H^{r+1}(\Omega) \times H^{r+1}(\Omega)$ onto $V_h^r \times V_h^r$, and it will be specified in the analysis. It is often, but not necessarily, a projection, and will be judiciously chosen in the error estimates when different numerical fluxes are used in the scheme.

In the analysis, a specifically designed operator Π_h turns out to be crucial. It is defined as

$$\Pi_h \begin{pmatrix} B \\ E \end{pmatrix} = \begin{pmatrix} \Pi_h^B(B,E) \\ \Pi_h^E(E,B) \end{pmatrix} = \begin{pmatrix} P_h^+((\frac{1}{2}+\alpha)B + \beta_1 E) + P_h^-((\frac{1}{2}-\alpha)B - \beta_1 E) \\ P_h^+((\frac{1}{2}-\alpha)E + \beta_2 B) + P_h^-((\frac{1}{2}+\alpha)E - \beta_2 B) \end{pmatrix}, \tag{2.17}$$

for any parameter $\alpha, \beta_1, \beta_2 \in \mathbb{R}$. The properties of Π_h will be summarized in the following Lemma.

Lemma 2.4. *For any given $\alpha, \beta_1, \beta_2 \in \mathbb{R}$, Π_h in (2.17), as an operator from $H^{r+1}(\Omega) \times H^{r+1}(\Omega)$ onto $V_h^r \times V_h^r$, has the following properties:*

$(i) \quad \displaystyle\int_{I_j} \eta_B \phi_x dx = 0, \quad \int_{I_j} \eta_E \psi_x dx = 0, \qquad \forall \phi, \psi \in V_h^r, \quad \forall j,$ \hfill (2.18)

$(ii) \quad \left\| \begin{pmatrix} B \\ E \end{pmatrix} - \Pi_h \begin{pmatrix} B \\ E \end{pmatrix} \right\| \le C_\star \left(1 + |\alpha| + \max(|\beta_1|, |\beta_2|) \right) h^{r+1} (\|B\|_{H^{r+1}} + \|E\|_{H^{r+1}}).$ \hfill (2.19)

If we further assume $\alpha^2 + \beta_1 \beta_2 = \frac{1}{4}$, then

$(iii) \quad \Pi_h \text{ defines a projection, namely } \Pi_h^2 = \Pi_h,$ \hfill (2.20)

$(iv) \quad \mathcal{F}_B(\eta_B, \eta_E)_{j-\frac{1}{2}} = 0, \quad \mathcal{F}_E(\eta_E, \eta_B)_{j-\frac{1}{2}} = 0, \forall j.$ \hfill (2.21)

Proof. First of all, Π_h is linear, and it is also onto $V_h^r \times V_h^r$ since P_h^+ and P_h^- are invariant on V_h^r.

The equalities in (i) are straightforward results from the definitions and the linearity of $P_h^\pm$ in (2.13) and (2.14), and the proof will be omitted. In order to show the results in (ii), we only need to estimate $\|B - \Pi_h^B(B, E)\|$ due to similarity to the other term.

$$\|B - \Pi_h^B(B, E)\| = \|(I - P_h^+)((\tfrac{1}{2} + \alpha)B + \beta_1 E) + (I - P_h^-)((\tfrac{1}{2} - \alpha)B - \beta_1 E)\|$$
$$\le C_\star(1 + |\alpha| + |\beta_1|)h^{r+1}(\|B\|_{H^{r+1}} + \|E\|_{H^{r+1}}). \tag{2.22}$$

In the last inequality, we have applied the approximation property of $P_h^\pm$ in (2.15). Here and below I denotes the identity operator.

From now on, we assume $\alpha^2 + \beta_1 \beta_2 = \frac{1}{4}$, and will establish the properties $(iii) - (iv)$. To show Π_h is a projection, namely $\Pi_h^2 = \Pi_h$, we follow the definition of Π_h and get

$$\Pi_h^2 \begin{pmatrix} B \\ E \end{pmatrix} = \begin{pmatrix} P_h^+((\tfrac{1}{2} + \alpha)\Pi_h^B(B, E) + \beta_1 \Pi_h^E(E, B)) + P_h^-((\tfrac{1}{2} - \alpha)\Pi_h^B(B, E) - \beta_1 \Pi_h^E(E, B)) \\ P_h^+((\tfrac{1}{2} - \alpha)\Pi_h^E(E, B) + \beta_2 \Pi_h^B(B, E)) + P_h^-((\tfrac{1}{2} + \alpha)\Pi_h^E(E, B) - \beta_2 \Pi_h^B(B, E)) \end{pmatrix}.$$
\hfill (2.23)

Now we will show the first component on the right of (2.23) is indeed $\Pi_h^B(B, E)$. With the definition of Π_h, we have

$$P_h^+ \left((\tfrac{1}{2} + \alpha)\Pi_h^B(B, E) + \beta_1 \Pi_h^E(E, B) \right)$$
$$= (P_h^+)^2 \left((\tfrac{1}{4} + \alpha + \alpha^2 + \beta_1 \beta_2)B + \beta_1 E \right) + P_h^+ P_h^- \left((\tfrac{1}{4} - \alpha^2 - \beta_1 \beta_2)B \right).$$

We then utilize that P_h^+ is a projection, namely $(P_h^+)^2 = P_h^+$, and the relation $\alpha^2 + \beta_1 \beta_2 = \frac{1}{4}$, to get

$$P_h^+ \left((\tfrac{1}{2} + \alpha)\Pi_h^B(B, E) + \beta_1 \Pi_h^E(E, B) \right) = P_h^+ \left((\tfrac{1}{2} + \alpha)B + \beta_1 E \right). \tag{2.24}$$

With similar arguments, we obtain

$$P_h^- \left((\tfrac{1}{2} - \alpha)\Pi_h^B(B, E) - \beta_1 \Pi_h^E(E, B) \right) = P_h^+ \left((\tfrac{1}{2} - \alpha)B - \beta_1 E \right). \tag{2.25}$$

Combining (2.24) and (2.25), we conclude that the first component of (2.23) is indeed $\Pi_h^B(B, E)$. Similarly, one can show that the second component of (2.23) is $\Pi_h^E(E, B)$.

Finally we will prove (iv). Due to similarity we will only show $\mathcal{F}_B(\eta_B, \eta_E) = 0$. Here the subscript $j - \frac{1}{2}$ is omitted for the simplicity of notation. With the linearity and the consistency of the numerical flux, we have

$$\begin{aligned}
\mathcal{F}_B(\eta_B, \eta_E) &= \mathcal{F}_B(B, E) - \mathcal{F}_B(\Pi_h^B(B, E), \Pi_h^E(E, B)) \\
&= B - \mathcal{F}_B(\Pi_h^B(B, E), \Pi_h^E(E, B)).
\end{aligned} \tag{2.26}$$

Based on definitions of Π_h^B and Π_h^E as well as the jump $[\cdot]$ and average $\{\cdot\}$, one has

$$\begin{aligned}
\mathcal{F}_B(\Pi_h^B(B, E), \Pi_h^E(E, B)) &= \{\Pi_h^B(B, E)\} + \alpha[\Pi_h^B(B, E)] + \beta_1[\Pi_h^E(E, B)] \\
&= \left(P_h^+ \left((\frac{1}{2} + \alpha)((\frac{1}{2} + \alpha)B + \beta_1 E) + \beta_1((\frac{1}{2} - \alpha)E + \beta_2 B) \right) \right)^+ \\
&+ \left(P_h^+ \left((\frac{1}{2} - \alpha)((\frac{1}{2} + \alpha)B + \beta_1 E) - \beta_1((\frac{1}{2} - \alpha)E + \beta_2 B) \right) \right)^- \\
&+ \left(P_h^- \left((\frac{1}{2} + \alpha)((\frac{1}{2} - \alpha)B - \beta_1 E) + \beta_1((\frac{1}{2} + \alpha)E - \beta_2 B) \right) \right)^+ \\
&+ \left(P_h^- \left((\frac{1}{2} - \alpha)((\frac{1}{2} - \alpha)B - \beta_1 E) - \beta_1((\frac{1}{2} + \alpha)E - \beta_2 B) \right) \right)^-.
\end{aligned}$$

Let each row of the right hand side of this equation be denoted as Λ_i, $i = 1, \ldots, 4$. With the property of $P_h^{\pm}$, particularly $(P_h^+ w)^+ = w$, $(P_h^- w)^- = w$ at a grid point where $w \in H^{r+1}(\Omega)$ is single-valued, we can simplify the sum of the first and the fourth terms,

$$\begin{aligned}
\Lambda_1 + \Lambda_4 =& (\frac{1}{2} + \alpha)((\frac{1}{2} + \alpha)B + \beta_1 E) + \beta_1((\frac{1}{2} - \alpha)E + \beta_2 B) \\
&+ (\frac{1}{2} - \alpha)((\frac{1}{2} - \alpha)B - \beta_1 E) - \beta_1((\frac{1}{2} + \alpha)E - \beta_2 B) = 2(\frac{1}{4} + \alpha^2 + \beta_1 \beta_2)B. \tag{2.27}
\end{aligned}$$

Moreover, one can easily show that

$$\Lambda_2 = (\frac{1}{4} - \alpha^2 - \beta_1 \beta_2)(P_h^+ B)^-, \qquad \Lambda_3 = (\frac{1}{4} - \alpha^2 - \beta_1 \beta_2)(P_h^- B)^+. \tag{2.28}$$

Combining (2.26), (2.27) and (2.28), we have

$$\begin{aligned}
\mathcal{F}_B(\eta_B, \eta_E) &= B - \mathcal{F}_B(\Pi_h^B(B, E), \Pi_h^E(E, B)) = B - \sum_{i=1}^{4} \Lambda_i \\
&= (\frac{1}{4} - \alpha^2 - \beta_1 \beta_2)\left(((I - P_h^+)B)^- + ((I - P_h^-)B)^+ \right). \tag{2.29}
\end{aligned}$$

Finally using the relation $\alpha^2 + \beta_1 \beta_2 = \frac{1}{4}$, we can conclude $\mathcal{F}_B(\eta_B, \eta_E) = 0$. $\square$

Now we are ready to state and establish the L^2 error estimates of the proposed DG methods.

Theorem 2.5. *For the semi-discrete DG method (2.2) (or (2.3)) with the numerical flux (2.5), $\beta_i \geq 0$, $i = 1, 2$, and the L^2-type initialization with $B_h(0, \cdot) = P_h B(0, \cdot)$, $E_h(0, \cdot) = P_h E(0, \cdot)$, the following error estimates hold when the exact solutions have sufficient regularity.*

(i) In general, when $\min(\beta_1, \beta_2) > 0$, we have

$$\|e_h\| \leq Ch^{r+\frac{1}{2}} \left(\max_{i=1,2} \frac{1 + |\alpha| + \beta_i}{\sqrt{\beta_i}} + h^{\frac{1}{2}} \right) \leq Ch^{r+\frac{1}{2}}, \tag{2.30}$$

8

and when $\beta_1\beta_2 = 0$, we have

$$\|e_h\| \le C(1 + |\alpha| + \max(\beta_1, \beta_2))h^r. \tag{2.31}$$

(ii) When an $\alpha\beta$-flux with $\alpha^2 + \beta_1\beta_2 = \frac{1}{4}$ is used in the DG method (2.2) (or (2.3)), we have

$$\|e_h\| \le C(1 + |\alpha| + \max(\beta_1, \beta_2))\, h^{r+1}. \tag{2.32}$$

The generic constant C above is independent of h. It may depend on the mesh parameter σ, and the H^{r+1}-norm of B, E, B_t, and E_t up to time T.

Proof. With the numerical flux (2.5) being consistent, the proposed scheme is consistent, therefore the exact solutions E and B satisfy

$$a_h(E, B; \phi, \psi) = \mathcal{S}(\phi), \qquad \forall \phi, \psi \in V_h^r.$$

This, together with the numerical scheme (2.3) and the linearity of a_h with respect to each argument, gives the error equation,

$$a_h(e_E, e_B; \phi, \psi) = 0, \qquad \forall \phi, \psi \in V_h^r. \tag{2.33}$$

We now take $\phi = \zeta_E$ and $\psi = \zeta_B$ in (2.33) and obtain

$$a_h(\zeta_E, \zeta_B; \zeta_E, \zeta_B) = -a_h(\eta_E, \eta_B; \zeta_E, \zeta_B). \tag{2.34}$$

Since ζ_E, ζ_B are in V_h^r, one can use (2.11) to rewrite the term on the left,

$$a_h(\zeta_E, \zeta_B; \zeta_E, \zeta_B) = \frac{1}{2}\frac{d}{dt}\int_\Omega \left(\zeta_E^2 + \zeta_B^2\right) dx + \sum_j \left(\beta_1[\zeta_E]^2 + \beta_2[\zeta_B]^2\right)_{j-\frac{1}{2}}. \tag{2.35}$$

For the term on the right in (2.34), based on the definition of a_h, we have

$$-a_h(\eta_E, \eta_B; \zeta_E, \zeta_B) = -\int_\Omega (\eta_E)_t \zeta_E dx - \sum_j \left(\int_{I_j} \eta_B(\zeta_E)_y dx + (\mathcal{F}_B(\eta_B, \eta_E)[\zeta_E])_{j-\frac{1}{2}}\right)$$
$$- \int_\Omega (\eta_B)_t \zeta_B dx - \sum_j \left(\int_{I_j} \eta_E(\zeta_B)_y dx + (\mathcal{F}_E(\eta_E, \eta_E)[\zeta_B])_{j-\frac{1}{2}}\right). \tag{2.36}$$

In the following, we will estimate (2.36) for the DG methods with different numerical fluxes as stated in (i) and (ii), separately. One of the keys is to properly choose the operator π_h to define η_h and ζ_h.

For the methods in (i), we take π_h as the L^2 projection, namely,

$$\pi_h \begin{pmatrix} B \\ E \end{pmatrix} = \begin{pmatrix} P_h B \\ P_h E \end{pmatrix}.$$

Therefore, ζ_E and ζ_B will be zero at $t = 0$, and

$$-a_h(\eta_E, \eta_B; \zeta_E, \zeta_B) = -\sum_j \left(\mathcal{F}_B(\eta_B, \eta_E)[\zeta_E] + \mathcal{F}_E(\eta_E, \eta_B)[\zeta_B]\right)_{j-\frac{1}{2}}. \tag{2.37}$$

9

When $\min(\beta_1, \beta_2) > 0$, we also have

$$-\sum_j \Big(\mathcal{F}_B(\eta_B, \eta_E)[\zeta_E] + \mathcal{F}_E(\eta_E, \eta_B)[\zeta_B]\Big)_{j-\frac{1}{2}}$$

$$\leq \frac{1}{2}\sum_j \Big(\beta_1[\zeta_E]^2 + \beta_2[\zeta_B]^2\Big)_{j-\frac{1}{2}} + \frac{1}{2}\sum_j \Big(\frac{1}{\beta_1}(\mathcal{F}_B(\eta_B, \eta_E))^2 + \frac{1}{\beta_2}(\mathcal{F}_E(\eta_E, \eta_B))^2\Big)_{j-\frac{1}{2}}$$

$$\leq \frac{1}{2}\sum_j \Big(\beta_1[\zeta_E]^2 + \beta_2[\zeta_B]^2\Big)_{j-\frac{1}{2}} + C_\star \Big(\max_{i=1,2}\frac{(1+|\alpha|+\beta_i)^2}{\beta_i}\Big) h^{2r+1}(\|B\|^2_{H^{r+1}} + \|E\|^2_{H^{r+1}}), \quad (2.38)$$

with the approximation property (2.15) applied. Combining (2.34)-(2.38), we obtain

$$\frac{d}{dt}\int_I (\zeta_E^2 + \zeta_B^2)\, dx \leq C_\star \Big(\max_{i=1,2}\frac{(1+|\alpha|+\beta_i)^2}{\beta_i}\Big) h^{2r+1}(\|B\|^2_{H^{r+1}} + \|E\|^2_{H^{r+1}}).$$

This, along with the fact that ζ_E and ζ_B are zero at $t=0$, and α, β_1, β_2 are of $O(1)$, implies

$$\|\zeta_E(\cdot, t)\|^2 + \|\zeta_B(\cdot, t)\|^2 \leq C\Big(\max_{i=1,2}\frac{(1+|\alpha|+\beta_i)^2}{\beta_i}\Big) h^{2r+1} \leq Ch^{2r+1}. \quad (2.39)$$

Here the constant C depends on the mesh parameter σ, and $\|B\|_{H^{r+1}}$ and $\|E\|_{H^{r+1}}$ up to time T.

On the other hand, if $\beta_1\beta_2 = 0$, at least one of the jump terms in (2.35) vanishes, we use inverse inequality (2.16) and the approximation result (2.15) to get

$$-\sum_j \Big(\mathcal{F}_B(\eta_B, \eta_E)[\zeta_E] + \mathcal{F}_E(\eta_E, \eta_B)[\zeta_B]\Big)_{j-\frac{1}{2}}$$

$$\leq \Big(\frac{1}{h}\sum_j \big((\mathcal{F}_B(\eta_B, \eta_E))^2 + (\mathcal{F}_E(\eta_E, \eta_B))^2\big)_{j-\frac{1}{2}}\Big)^{\frac{1}{2}} \Big(h\sum_j([\zeta_E]^2 + [\zeta_B]^2)_{j-\frac{1}{2}}\Big)^{\frac{1}{2}}$$

$$\leq C_\star(1+|\alpha|+\max(\beta_1,\beta_2))h^r(\|B\|_{H^{r+1}} + \|E\|_{H^{r+1}})\left(\|\zeta_E\|^2 + \|\zeta_B\|^2\right)^{\frac{1}{2}}. \quad (2.40)$$

Combining (2.34)-(2.37) and (2.40), we get

$$\frac{d}{dt}\left(\|\zeta_E\|^2 + \|\zeta_B\|^2\right)^{\frac{1}{2}} \leq C_\star (1+|\alpha|+\max(\beta_1,\beta_2))\, h^r(\|B\|_{H^{r+1}} + \|E\|_{H^{r+1}}),$$

and therefore

$$\|\zeta_E(\cdot, t)\| + \|\zeta_B(\cdot, t)\| \leq C(1+|\alpha|+\max(\beta_1,\beta_2))h^r, \quad (2.41)$$

where the constant C depends on the mesh parameter σ, and $\|B\|_{H^{r+1}}$ and $\|E\|_{H^{r+1}}$ up to time T.

We now can apply the triangle inequality $\|e_h\| \leq \|\eta_h\| + \|\zeta_h\|$ and the approximation property of $\pi_h = P_h$ in (2.15) to conclude the estimates in (2.30) and (2.31).

We next turn to the DG method in (ii) with an $\alpha\beta$-flux, namely, the flux in (2.5) with α, β_1, β_2 satisfying $\alpha^2 + \beta_1\beta_2 = \frac{1}{4}$ and $\beta_i \geq 0$, $i = 1, 2$. For this case, we choose π_h to be the projection Π_h defined in (2.17). Based on Lemma 2.4, (2.36) becomes

$$-a_h(\eta_E, \eta_B; \zeta_E, \zeta_B) = -\int_\Omega (\eta_E)_t \zeta_E dx - \int_\Omega (\eta_B)_t \zeta_B dx$$

$$\leq C_\star(1+|\alpha|+\max(\beta_1,\beta_2))h^{r+1}(\|B_t\|_{H^{r+1}} + \|E_t\|_{H^{r+1}})\left(\|\zeta_E\|^2 + \|\zeta_B\|^2\right)^{\frac{1}{2}}. \quad (2.42)$$

10

Here we have applied the approximation property in (2.19). Combining (2.34)-(2.37) and (2.42), as well as the initial error,

$$\left\| \Pi_h \begin{pmatrix} B \\ E \end{pmatrix} - \begin{pmatrix} B_h \\ E_h \end{pmatrix} \right\|_{t=0} = \left\| \Pi_h \begin{pmatrix} B \\ E \end{pmatrix} - \begin{pmatrix} B \\ E \end{pmatrix} + \begin{pmatrix} B \\ E \end{pmatrix} - \begin{pmatrix} P_h B \\ P_h E \end{pmatrix} \right\|_{t=0}$$

$$\leq C_\star (1 + |\alpha| + \max(\beta_1, \beta_2)) h^{r+1} (\|B\|_{H^{r+1}} + \|E\|_{H^{r+1}})|_{t=0}, \quad (2.43)$$

we obtain

$$\|\zeta_E(\cdot, t)\| + \|\zeta_B(\cdot, t)\| \leq C_\star (1 + |\alpha| + \max(\beta_1, \beta_2)) h^{r+1} + \|\zeta_E(\cdot, 0)\| + \|\zeta_B(\cdot, 0)\|$$

$$\leq C(1 + |\alpha| + \max(\beta_1, \beta_2)) h^{r+1}.$$

Here the constant C depends on the mesh parameter σ, and $\|B_t\|_{H^{r+1}}$ and $\|E_t\|_{H^{r+1}}$ up to time T, and it also depends on $\|B\|_{H^{r+1}}$ and $\|E\|_{H^{r+1}}$ at $t = 0$.

Finally we apply the triangle inequality and the approximation property of $\pi_h = \Pi_h$ in Lemma 2.4 to conclude the estimate in (2.32) when an $\alpha\beta$-flux is used in the proposed method. □

In Theorem 2.5, the initialization is through L^2 projection. Some other initialization strategies can also be used without changing the orders of accuracy established for the proposed methods. Among the general numerical flux (2.5), some lead to sub-optimal estimates. One such example, with which the accuracy is confirmed to be sharp numerically, is the central flux ($\alpha = \beta_1 = \beta_2 = 0$) with k being odd. On the other hand, our analysis shows that $\alpha\beta$-fluxes will result in DG methods with optimal accuracy (this is with respect to the approximation property of V_h^r); note again that this family of numerical fluxes include the upwind and alternating fluxes. With a close examination of the proof, one will see that the condition to define the $\alpha\beta$-fluxes, namely $\alpha^2 + \beta_1\beta_2 = \frac{1}{4}$, can indeed be further relaxed without compromising the optimal accuracy of the DG methods. This generalization is summarized in the next theorem.

Theorem 2.6. *Consider the numerical flux (2.5), where α, β_1, β_2 satisfy*

$$\alpha^2 + \beta_1\beta_2 = \frac{1}{4} + ch^\delta \geq 0, \qquad \beta_i \geq 0, \;\; i = 1, 2 \tag{2.44}$$

where c is a constant independent of h,

$$\delta \geq \frac{1}{2} \;\; \text{when } \min(\beta_1, \beta_2) > 0; \quad \delta \geq 1 \;\; \text{when } \beta_1\beta_2 = 0. \tag{2.45}$$

When such numerical flux is used in the semi-discrete DG method (2.2) (or (2.3)) with the L^2-type initialization $B_h(0, \cdot) = P_h B(0, \cdot)$, $E_h(0, \cdot) = P_h E(0, \cdot)$, the method will have optimal error estimate as follows.

$$\|e_h\| \leq \begin{cases} C\left(\frac{(1+|\alpha|+\max(\beta_1,\beta_2))}{\min(\beta_1,\beta_2,1)}\right) h^{r+1}, & \min(\beta_1, \beta_2) > 0, \\ C\left(1 + |\alpha| + \max(\beta_1, \beta_2)\right) h^{r+1}, & \beta_1\beta_2 = 0. \end{cases} \tag{2.46}$$

The generic constant C above is independent of h. It may depend on c, the mesh parameter σ, and the H^{r+1}-norm of B, E, B_t, and E_t up to time T.

Proof. The proof will be based on some modification of that for Theorem 2.5 and of some results in Lemma 2.4. We briefly illustrate the main steps in the following.

Step 1. First, we consider the operator Π_h defined in (2.17) with α, β_1, β_2 satisfying (2.44)-(2.45). Although this operator is no longer a projection, it still has the properties $(i) - (ii)$ in Lemma 2.4. The property (iv) in Lemma 2.4 is now replaced by

$$(iv') \quad \mathcal{F}_B(\eta_B, \eta_E)_{j-\frac{1}{2}} = C_\star h^{r+\frac{1}{2}+\delta} \|B\|_{H^{r+1}}, \quad \mathcal{F}_E(\eta_E, \eta_B)_{j-\frac{1}{2}} = C_\star h^{r+\frac{1}{2}+\delta} \|E\|_{H^{r+1}}, \ \forall j, \quad (2.47)$$

and this is a direct result of (2.29) and its counterpart for $\mathcal{F}_E(\eta_E, \eta_B)_{j-\frac{1}{2}}$, together with the approximation property of $P_h^\pm$ in (2.15).

Step 2. For the error estimate, we can follow the arguments in the beginning of the proof of Theorem 2.5 and get (2.34)-(2.36). We then define η_h and ζ_h by specifying π_h as the operator Π_h in (2.17), and get

$$-a_h(\eta_E, \eta_B; \zeta_E, \zeta_B) = - \int_\Omega (\eta_E)_t \zeta_E + (\eta_B)_t \zeta_B dx$$
$$- \sum_j \left(\mathcal{F}_B(\eta_B, \eta_E)[\zeta_E] + \mathcal{F}_E(\eta_E, \eta_E)[\zeta_B] \right)_{j-\frac{1}{2}}. \quad (2.48)$$

The first term on the right-hand side has been estimated in (2.42),

$$- \int_\Omega (\eta_E)_t \zeta_E + (\eta_B)_t \zeta_B dx \le C_\star (1 + \alpha + \max(\beta_1, \beta_2)) h^{r+1} (\|B_t\|_{H^{r+1}} + \|E_t\|_{H^{r+1}}) \left(\|\zeta_E\|^2 + \|\zeta_B\|^2 \right)^{\frac{1}{2}}.$$
$$(2.49)$$

As for the second term on the right, based on (2.38)-(2.40) and (2.47), we get

$$- \sum_j ((\mathcal{F}_B(\eta_B, \eta_E)[\zeta_E] + (\mathcal{F}_E(\eta_E, \eta_B)[\zeta_B])_{j-\frac{1}{2}}$$

$$\le \begin{cases} \frac{\beta}{2} \sum_j ([\zeta_E]_{j-\frac{1}{2}}^2 + [\zeta_B]_{j-\frac{1}{2}}^2) + C_\star \left(\max_{i=1,2} \frac{(1+|\alpha|+\beta_i)^2}{\beta_i} \right) h^{2r+1+2\delta} (\|B\|_{H^{r+1}}^2 + \|E\|_{H^{r+1}}^2), & \min(\beta_1, \beta_2) > 0 \\ C_\star (1 + |\alpha| + \max(\beta_1, \beta_2)) h^{r+\delta} (\|B\|_{H^{r+1}} + \|E\|_{H^{r+1}}) \left(\|\zeta_E\|^2 + \|\zeta_B\|^2 \right)^{\frac{1}{2}}, & \beta_1 \beta_2 = 0. \end{cases}$$
$$(2.50)$$

Now we can combine (2.34)-(2.36), (2.48)-(2.50), the choice of the parameter δ in (2.45), and the initial error in (2.43) to conclude the optimal error estimate (2.46). $\qquad\square$

Remark 2.7. *When the wave problem in (1.1) is free of the source terms, one can further show that the constant C in the error estimates in Theorems 2.5 and 2.6 will depend on time T at most linearly, see also Figures 3.1-3.2 in Section 3.*

Remark 2.8. *With the more general numerical flux (2.8) with $\beta_i \ge 0$, $i = 1, 2$, it can be shown that $\|e_h\| \le Ch^{r+\frac{1}{2}}$ when $4\beta_1 \beta_2 > (\alpha_1 + \alpha_2)^2$, and $\|e_h\| \le Ch^r$ when $4\beta_1 \beta_2 = (\alpha_1 + \alpha_2)^2$. The DG methods with the $\alpha\beta$-fluxes defined in (2.5) and (2.7), or its generalization as in (2.44), are still all we have identified to be L^2 optimal through the current framework using a local projection operator (2.17) in the analysis, see also the brief comment in Section 4 on a global projection operator.*

2.3 Superconvergence and accuracy enhancement

In this subsection, we study the superconvergence properties of the DG methods with $\alpha\beta$-fluxes. For the general L^2 stable DG methods, postprocessing techniques are presented to gain extra accuracy.

Superconvergence property is observed in the numerical solutions of some DG schemes, and theoretical analysis has been carried out in literature, see [34, 6] for recent work on one-dimensional linear advection equation. For the DG methods with $\alpha\beta$-fluxes and under suitable initial discretization, we will establish the $(r+2)$-th order superconvergence rate of the DG approximation towards a special projection of the exact solution in the L^2 norm as well as in a specially defined L^∞-type norm (see (2.52)), and of the L^2 norm of the cell average of the solution errors.

The first step to obtain the superconvergence property is to carefully choose the numerical initial conditions. Related to this, we have the following lemma.

Lemma 2.9. *Based on the initial condition $E(0,\cdot)$, $B(0,\cdot)$, there exist numerical initial discretizations, denoted by $E_h(0,\cdot)$, $B_h(0,\cdot)$, such that the following properties are satisfied at time $t = 0$:*

$$(\zeta_B)_t = 0, \quad (\zeta_E)_t = 0,$$
$$\|\zeta_B\| \le Ch^{r+2}, \quad \|\zeta_E\| \le Ch^{r+2}. \tag{2.51}$$

Here π_h is taken as Π_h in (2.17) to define $\zeta_h = (\zeta_B, \zeta_E)^\top$.

We would like to comment that the construction of such initial discretization is highly non-trivial and we refer to [34] for the details how to compute it, as well as the proof of Lemma 2.9. On the other hand, this special initialization is sufficient yet not always necessary for the numerical solutions by DG methods with $\alpha\beta$-flux to display the type of superconvergence properties summarized in next theorem, see Section 3 for some numerical examples. Now we are ready to state the main theorem.

Theorem 2.10. *For the semi-discrete DG method (2.2) (or (2.3)) with an $\alpha\beta$-flux (2.7) and a numerical initial discretization as prescribed in Lemma 2.9, when the exact solutions have sufficient regularity, the following estimates will hold at the time $t = T$,*

$$\left(\frac{1}{N} \sum_{j=1}^{N} \left(|\zeta_E(y_j)|^2 + |\zeta_B(y_j)|^2 \right) \right)^{\frac{1}{2}} \le Ch^{r+2}, \tag{2.52}$$

$$\|\bar{e}_B\| + \|\bar{e}_E\| \le Ch^{r+2}, \tag{2.53}$$

$$\|\zeta_B\| + \|\zeta_E\| \le Ch^{r+2}. \tag{2.54}$$

Here π_h is taken as Π_h in (2.17) to define $\zeta_h = (\zeta_B, \zeta_E)^\top$, and y_j is any point in the cell I_j with the same reference position, i.e., $y_j = x_j + ah_j$ with a independent of j. The constant C is independent of h, and may depend on r, α, β and some Sobolev norms of the exact solution E and B up to time T.

The proof follows the framework introduced by Yang and Shu [34], where they prove similar results for the linear scalar hyperbolic equation with the upwind flux. We extend their results to the linear hyperbolic system and for more general choice of numerical fluxes. As the main structure of the proof follows that in [34], we shall only highlight the main steps and point out the key differences (mostly related to the use of the $\alpha\beta$-flux) in the following analysis.

Proof. Step 1: Let $\bar{\zeta}_q$ define the cell average of ζ_q in each cell I_j, namely, $\bar{\zeta}_q|_{I_j} = \frac{1}{h_j}\int_{I_j}\zeta_q dx$, $\forall j = 1, \cdots, N$, where q can be either E or B, then we have

$$\|\zeta_E - \bar{\zeta}_E\|_{I_j} + \|\zeta_B - \bar{\zeta}_B\|_{I_j} \le Ch_j \left(\|(\zeta_E)_x\|_{I_j} + \|(\zeta_B)_x\|_{I_j} \right) \tag{2.55}$$

based on Friedrichs' inequality. Here $\|\cdot\|_{I_j}$ denotes the L^2 norm in I_j.

13

For the DG method with an $\alpha\beta$-flux and the projection $\pi_h = \Pi_h$ as defined in (2.17), the error equations take the form

$$\int_{I_j} (e_E)_t \phi dx + \int_{I_j} \zeta_B \phi_x dx - (\mathcal{F}_B(\zeta_B, \zeta_E)\phi^-)_{j+\frac{1}{2}} + (\mathcal{F}_B(\zeta_B, \zeta_E)\phi^+)_{j-\frac{1}{2}} = 0, \tag{2.56a}$$

$$\int_{I_j} (e_B)_t \psi dx + \int_{I_j} \zeta_E \psi_x dx - (\mathcal{F}_E(\zeta_E, \zeta_B)\psi^-)_{j+\frac{1}{2}} + (\mathcal{F}_E(\zeta_E, \zeta_B)\psi^+)_{j-\frac{1}{2}} = 0, \tag{2.56b}$$

for all test functions $\phi,\, \psi \in V_h^r$, and for all j. Utilizing the relation $\alpha^2 + \beta_1\beta_2 = \frac{1}{4}$, we can obtain

$$\int_{I_j} \left(-\beta_2 e_E + (\frac{1}{2} + \alpha)e_B \right)_t \phi dx$$
$$- \int_{I_j} \left((\frac{1}{2} + \alpha)\zeta_E - \beta_2\zeta_B \right)_x \phi dx - \left(((\frac{1}{2} + \alpha)[\zeta_E] - \beta_2[\zeta_B])\phi^+ \right)_{j-\frac{1}{2}} = 0, \tag{2.57}$$

$$\int_{I_j} \left((\frac{1}{2} + \alpha)e_E + \beta_1 e_B \right)_t \psi dx$$
$$- \int_{I_j} \left(\beta_1\zeta_E + (\frac{1}{2} + \alpha)\zeta_B \right)_x \psi dx - \left((\beta_1[\zeta_E] + (\frac{1}{2} + \alpha)[\zeta_B])\psi^- \right)_{j+\frac{1}{2}} = 0. \tag{2.58}$$

When $\frac{1}{2} + \alpha \neq 0$, we can see

$$\det \begin{bmatrix} \frac{1}{2} + \alpha & \beta_1 \\ -\beta_2 & \frac{1}{2} + \alpha \end{bmatrix} = \frac{1}{2} + \alpha \neq 0, \tag{2.59}$$

and then

$$\|(\zeta_E)_x\|_{I_j} + \|(\zeta_B)_x\|_{I_j} \leq C \left(\left\| ((\frac{1}{2} + \alpha)\zeta_E - \beta_2\zeta_B)_x \right\|_{I_j} + \left\| (\beta_1\zeta_E + (\frac{1}{2} + \alpha)\zeta_B)_x \right\|_{I_j} \right)$$
$$\leq C \left(\left\| P_h \left(-\beta_2 e_E + (\frac{1}{2} + \alpha)e_B \right)_t \right\|_{I_j} + \left\| P_h \left((\frac{1}{2} + \alpha)e_E + \beta_1 e_B \right)_t \right\|_{I_j} \right)$$
$$\leq C \left(\|P_h(e_B)_t\|_{I_j} + \|P_h(e_E)_t\|_{I_j} \right) \leq C \left(\|(e_B)_t\|_{I_j} + \|(e_E)_t\|_{I_j} \right). \tag{2.60}$$

Here the first inequality is due to (2.59), and the second inequality is derived from (2.57)-(2.58) with essentially the same analysis as in [34, Lemma 3.6]. When $\frac{1}{2} + \alpha = 0$, the same result $\|(\zeta_E)_x\|_{I_j} + \|(\zeta_B)_x\|_{I_j} \leq C(\|(e_B)_t\|_{I_j} + \|(e_E)_t\|_{I_j})$ can be concluded if we work with the next two equalities instead

$$\int_{I_j} \left((\frac{1}{2} - \alpha)e_E - \beta_1 e_B \right)_t \phi dx$$
$$- \int_{I_j} \left(-\beta_1\zeta_E + (\frac{1}{2} - \alpha)\zeta_B \right)_x \phi dx - \left((-\beta_1[\zeta_E] + (\frac{1}{2} - \alpha)[\zeta_B])\phi^- \right)_{j+\frac{1}{2}} = 0, \tag{2.61}$$

$$\int_{I_j} \left(\beta_2 e_E + (\frac{1}{2} - \alpha)e_B \right)_t \psi dx$$
$$- \int_{I_j} \left((\frac{1}{2} - \alpha)\zeta_E + \beta_2\zeta_B \right)_x \psi dx - \left(((\frac{1}{2} - \alpha)[\zeta_E] + \beta_2[\zeta_B])\psi^+ \right)_{j-\frac{1}{2}} = 0. \tag{2.62}$$

14

One can further estimate $\|(e_B)_t\|$ and $\|(e_E)_t\|$ following a similar analysis as in Theorem 2.5 to bound $\|e_B\|$ and $\|e_E\|$. We skip the details and only state the result.

$$\|(e_B)_t\| + \|(e_E)_t\| \leq Ch^{r+1}. \tag{2.63}$$

With this and (2.55), (2.60), we have

$$\|\zeta_E - \bar{\zeta}_E\| + \|\zeta_B - \bar{\zeta}_B\| \leq Ch^{r+2}. \tag{2.64}$$

Step 2: Next, we proceed to estimate $\zeta_h(y_j)$ as well as $\|\bar{\zeta}_h\|$. For any point y_j in the cell I_j, we can construct a unique set of $r+1$ quadrature points in I_j, denoted as $\{\hat{x}_j^i\}_{0 \leq i \leq r}$, which includes $y_j (= \hat{x}_j^i$ for some index i) and at the same time is accurate for the integration of polynomials of degree $2r$ over I_j. Let the corresponding weights on a reference element $[-1, 1]$ be $\{w_i\}_{0 \leq i \leq r}$. In addition, let $\chi_j^i \in V_h^r$ be a piecewise polynomial of degree r, which is nonzero only in I_j and satisfies $\chi_j^i(x_j^{i'}) = \delta_{i,i'}$. Here $\delta_{i,i'}$ is Kronecker delta function. With this, we have $\zeta_h(y_j) = \zeta_h(\hat{x}_j^i) = \frac{2}{w_i h_j} \int_{I_j} \zeta_h \chi_j^i dx = \frac{2}{w_i h_j} \int_\Omega \zeta_h \chi_j^i dx$. From now on, we will use the notation $(u, v) = \int_\Omega uv dx$.

Let's consider the following dual problem:

$$\begin{aligned}
(\phi_j)_t - (\phi_j)_x &= 0, \quad (x,t) \in [a,b] \times (0,T], \\
\phi_j(x,T) &= \chi_j^i(x), \quad x \in [a,b], \\
\phi_j(a,t) &= \phi_j(b,t), \quad t \in (0,T].
\end{aligned}$$

We now introduce the following projections of ϕ_j:

$$P_h^{(1)} \phi_j = \left(\frac{1}{2} - \alpha - \beta_2\right) P_h^+ \phi_j + \left(\frac{1}{2} + \alpha + \beta_2\right) P_h^- \phi_j, \tag{2.65}$$

$$P_h^{(2)} \phi_j = \left(\frac{1}{2} + \alpha - \beta_1\right) P_h^+ \phi_j + \left(\frac{1}{2} - \alpha + \beta_1\right) P_h^- \phi_j, \tag{2.66}$$

which mimic the definition of Π_h in (2.17).

Following [34], we have

$$(e_E(T), \chi_j^i) = (e_E, \phi_j)(T) = (e_E, \phi_j)(0) + \int_0^T \left(((e_E)_t, \phi_j) + (e_E, (\phi_j)_t)\right) dt, \tag{2.67}$$

and

$$((e_E)_t, \phi_j) + (e_E, (\phi_j)_t) = ((e_E)_t, \phi_j - P_h^{(1)}\phi_j) - H(\zeta_B, P_h^{(1)}\phi_j; \mathcal{F}_B(\zeta_B, \zeta_E)) + (\eta_E, (\phi_j)_x) + (\zeta_E, (\phi_j)_x),$$

where

$$\begin{aligned}
&H(\zeta_B, P_h^{(1)}\phi_j; \mathcal{F}_B(\zeta_B, \zeta_E)) \tag{2.68} \\
&= (\zeta_B, (P_h^{(1)}\phi_j)_x) + \sum_l \left(\mathcal{F}_B(\zeta_B, \zeta_E)[P_h^{(1)}\phi_j]\right)_{l-\frac{1}{2}} \\
&= -((\zeta_B)_x, P_h^{(1)}\phi_j) - \sum_l \left[\zeta_B P_h^{(1)}\phi_j\right]_{l-\frac{1}{2}} + \sum_l \left(\mathcal{F}_B(\zeta_B, \zeta_E)[P_h^{(1)}\phi_j]\right)_{l-\frac{1}{2}} \\
&= -((\zeta_B)_x, \phi_j) - \sum_l \left[\zeta_B P_h^{(1)}\phi_j\right]_{l-\frac{1}{2}} + \sum_l \left(\mathcal{F}_B(\zeta_B, \zeta_E)[P_h^{(1)}\phi_j]\right)_{l-\frac{1}{2}} \\
&= (\zeta_B, (\phi_j)_x) + \sum_l \left([\zeta_B \phi_j] - [\zeta_B P_h^{(1)}\phi_j] + \mathcal{F}_B(\zeta_B, \zeta_E)[P_h^{(1)}\phi_j]\right)_{l-\frac{1}{2}},
\end{aligned}$$

15

and the jump terms can be reorganized as

$$-[\zeta_B P_h^{(1)}\phi_j] + \mathcal{F}_B(\zeta_B,\zeta_E)[P_h^{(1)}\phi_j] = -[\zeta_B]\{P_h^{(1)}\phi_j\} + (\alpha[\zeta_B] + \beta_1[\zeta_E])[P_h^{(1)}\phi_j]$$
$$= -[\zeta_B](\{P_h^{(1)}\phi_j\} - \alpha[P_h^{(1)}\phi_j]) + \beta_1[\zeta_E][P_h^{(1)}\phi_j], \qquad (2.69)$$
$$[\zeta_B\phi_j] = [\zeta_B](\{\phi_j\} - (\alpha + \beta_2)[\phi_j]) + \{\zeta_B\}[\phi_j] + (\alpha + \beta_2)[\zeta_B][\phi_j]$$
$$= [\zeta_B](\{\phi_j\} - (\alpha + \beta_2)[\phi_j]) + (\{\zeta_B\} + (\alpha + \beta_2)[\zeta_B])[\phi_j]. \quad (2.70)$$

Similarly,

$$(e_B(T), \chi_j^i) = (e_B, \phi_j)(0) + \int_0^T \left(((e_B)_t, \phi_j) + (e_B, (\phi_j)_t) \right) dt, \qquad (2.71)$$

$$((e_B)_t, \phi_j) + (e_B, (\phi_j)_t) = ((e_B)_t, \phi_j - P_h^{(2)}\phi_j) - H(\zeta_E, P_h^{(2)}\phi_j; \mathcal{F}_E(\zeta_E,\zeta_B)) + (\eta_B, (\phi_j)_x) + (\zeta_B, (\phi_j)_x),$$

where

$$H(\zeta_E, P_h^{(2)}\phi_j; \mathcal{F}_E(\zeta_E,\zeta_B)) = (\zeta_E, (\phi_j)_x) + \sum_l \left([\zeta_E\phi_j] - [\zeta_E P_h^{(2)}\phi_j] + \mathcal{F}_E(\zeta_E,\zeta_B)[P_h^{(2)}\phi_j] \right)_{l-\frac{1}{2}},$$

and

$$-[\zeta_E P_h^{(2)}\phi_j] + \mathcal{F}_E(\zeta_E,\zeta_B)[P_h^{(2)}\phi_j] = -[\zeta_E](\{P_h^{(2)}\phi_j\} + \alpha[P_h^{(2)}\phi_j]) + \beta_2[\zeta_B][P_h^{(2)}\phi_j], \qquad (2.72)$$
$$[\zeta_E\phi_j] = [\zeta_E](\{\phi_j\} + (\alpha - \beta_1)[\phi_j]) + (\{\zeta_E\} - (\alpha - \beta_1)[\zeta_E])[\phi_j]. \quad (2.73)$$

Using the definitions of $P_h^{(1)}$ and $P_h^{(2)}$ in (2.65)-(2.66), as well as some simple algebra similar to the proof of Lemma 2.4, we can show

$$\{P_h^{(1)}\phi_j\} - \alpha[P_h^{(1)}\phi_j] - \beta_2[P_h^{(2)}\phi_j] = \left(\frac{1}{2} - \alpha - \beta_2 \right) \phi_j^+ + \left(\frac{1}{2} + \alpha + \beta_2 \right) \phi_j^-,$$

$$\{P_h^{(2)}\phi_j\} + \alpha[P_h^{(2)}\phi_j] - \beta_1[P_h^{(1)}\phi_j] = \left(\frac{1}{2} + \alpha - \beta_1 \right) \phi_j^+ + \left(\frac{1}{2} - \alpha + \beta_1 \right) \phi_j^-.$$

Then the sum of (2.69) and (2.72) becomes

$$- [\zeta_E P_h^{(2)}\phi_j] + \mathcal{F}_E(\zeta_E,\zeta_B)[P_h^{(2)}\phi_j] - [\zeta_B P_h^{(1)}\phi_j] + \mathcal{F}_B(\zeta_B,\zeta_E)[P_h^{(1)}\phi_j]$$
$$= -[\zeta_B] \left(\{P_h^{(1)}\phi_j\} - \alpha[P_h^{(1)}\phi_j] - \beta_2[P_h^{(2)}\phi_j] \right) - [\zeta_E] \left(\{P_h^{(2)}\phi_j\} + \alpha[P_h^{(2)}\phi_j] - \beta_1[P_h^{(1)}\phi_j] \right)$$
$$= -[\zeta_B] \left(\{\phi_j\} - (\alpha + \beta_2)[\phi_j] \right) - [\zeta_E] \left(\{\phi_j\} + (\alpha - \beta_1)[\phi_j] \right). \qquad (2.74)$$

This, together with (2.70) and (2.73), further gives

$$[\zeta_E\phi_j] - [\zeta_E P_h^{(2)}\phi_j] + \mathcal{F}_E(\zeta_E,\zeta_B)[P_h^{(2)}\phi_j] + [\zeta_B\phi_j] - [\zeta_B P_h^{(1)}\phi_j] + \mathcal{F}_B(\zeta_B,\zeta_E)[P_h^{(1)}\phi_j]$$
$$= (\{\zeta_B\} + (\alpha + \beta_2)[\zeta_B])[\phi_j] + (\{\zeta_E\} - (\alpha - \beta_1)[\zeta_E])[\phi_j]. \qquad (2.75)$$

16

Now we combine (2.67), (2.71), (2.75), and get

$$(e_E(T), \chi_j) + (e_B(T), \chi_j) = (e_E, \phi_j)(0) + (e_B, \phi_j)(0)$$

$$+ \int_0^T \Bigg(((e_E)_t, \phi_j - P_h^{(1)}\phi_j) + (\eta_E, (\phi_j)_x) - \sum_l \left((\{\zeta_B\} + (\alpha + \beta_2)[\zeta_B])[\phi_j] \right)_{l-\frac{1}{2}}$$

$$+ ((e_B)_t, \phi_j - P_h^{(2)}\phi_j) + (\eta_B, (\phi_j)_x) - \sum_l \left((\{\zeta_E\} - (\alpha - \beta_1)[\zeta_E])[\phi_j] \right)_{l-\frac{1}{2}} \Bigg) dt$$

$$= (e_E, \phi_j)(0) + (e_B, \phi_j)(0) + \int_0^T \left(((e_E)_t, \phi_j - P_h^{(1)}\phi_j) + ((e_B)_t, \phi_j - P_h^{(2)}\phi_j) \right) dt$$

$$+ \int_0^T \left((\eta_E, (\phi_j)_t) + (\eta_B, (\phi_j)_t) \right) dt, \tag{2.76}$$

For the last equality, we have used $\int_0^T \sum_l \left((\{\zeta_B\} + (\alpha + \beta_2)[\zeta_B])[\phi_j] \right)_{l-\frac{1}{2}} dt = 0$ and $\int_0^T \sum_l \left((\{\zeta_E\} - (\alpha - \beta_1)[\zeta_E])[\phi_j] \right)_{l-\frac{1}{2}} dt = 0$ which are due to that $[\phi_j]_{l-\frac{1}{2}} = 0$ except for a finite number of t. We further apply integration by parts to the last term of the right-hand side of (2.76), and get

$$(\zeta_E(T), \chi_j^i) + (\zeta_B(T), \chi_j^i) = (\zeta_E, \phi_j)(0) + (\zeta_B, \phi_j)(0) \tag{2.77}$$

$$+ \int_0^T \left(((e_E)_t, \phi_j - P_h^{(1)}\phi_j) + ((e_B)_t, \phi_j - P_h^{(2)}\phi_j) \right) dt - \int_0^T \left(((\eta_E)_t, \phi_j) + ((\eta_B)_t, \phi_j) \right) dt.$$

Using the characteristic lines of ϕ_j, Yang and Shu [34] performed a detailed analysis to bound some terms similar to those on the right-hand sides of (2.77). Following similar techniques, we can show

$$\sum_j (\Pi_1^j)^2 \le Ch^{2r+5}, \quad \text{where } \Pi_1^j := (\zeta_E, \phi_j)(0) + (\zeta_B, \phi_j)(0),$$

$$\sum_j (\Pi_2^j)^2 \le Ch^{2r+5}, \quad \text{where } \Pi_2^j := \int_0^T \left(((\eta_E)_t, \phi_j) + ((\eta_B)_t, \phi_j) \right) dt,$$

$$\sum_j (\Pi_3^j)^2 \le Ch^{2r+5}, \quad \text{where } \Pi_3^j := \int_0^T \left(((e_E)_t, \phi_j - P_h^{(1)}\phi_j) + ((e_B)_t, \phi_j - P_h^{(2)}\phi_j) \right) dt.$$

We refer the readers to [34] for more details. Now we gather all the estimates and obtain

$$\sum_j \left| (\zeta_E, \chi_j^i) + (\zeta_B, \chi_j^i) \right|^2 \le Ch^{2r+5}. \tag{2.78}$$

Step 3: Next, we consider another dual problem

$$\begin{aligned} (\psi_j)_t + (\psi_j)_x &= 0, \quad (x,t) \in [a,b] \times (0,T], \\ \psi_j(x,T) &= \chi_j^i(x), \quad x \in [a,b], \\ \psi_j(a,t) &= \psi_j(b,t), \quad t \in (0,T], \end{aligned}$$

and with a very similar analysis, we obtain

$$\sum_j \left| (\zeta_E, \chi_j^i) - (\zeta_B, \chi_j^i) \right|^2 \le Ch^{2r+5}. \tag{2.79}$$

17

The estimates in (2.78)-(2.79) readily imply

$$\sum_j \left|(\zeta_E, \chi_j^i)\right|^2, \quad \sum_j \left|(\zeta_B, \chi_j^i)\right|^2 \leq Ch^{2r+5}.$$

This means that, for any y_j in the cell I_j, we have

$$\frac{1}{N} \sum_j |\zeta_B(y_j)|^2 = \frac{1}{N} \sum_j \left|\frac{2}{w_i h_j}(\zeta_B, \chi_j^i)\right|^2 \leq Ch^{2r+4}, \tag{2.80}$$

$$\frac{1}{N} \sum_j |\zeta_E(y_j)|^2 \leq Ch^{2r+4}. \tag{2.81}$$

This leads to the superconvergence property (2.52).

Finally, we can carry out the analysis just as above, yet replacing χ_j^i in the two dual problems at time T by the indicator function of the cell I_j. This will yield

$$\|\bar{\zeta}_B\| + \|\bar{\zeta}_E\| \leq Ch^{r+2} \tag{2.82}$$

hence the estimate for the solution error e_h in (2.53). The superconvergence estimate (2.54) then follows from (2.64) and (2.82). $\qquad\square$

Remark 2.11. *The superconvergence results are proven for $\alpha\beta$-fluxes (2.7). When the numerical fluxes do not satisfy (2.7), we have tested the corresponding DG methods numerically, and no such superconvergence property has been observed.*

Finally we discuss an approach to gain extra accuracy through post-processing techniques using a specially designed convolution kernel. In [13], post-processing techniques are devised to enhance the accuracy for DG solutions on uniform meshes, and they are based on error estimates of even higher order accuracy in negative-order norms, namely,

$$\|u\|_{-l} = \sup_{0 \neq \phi \in C_0^\infty(\Omega)} \frac{\int_\Omega u(x)\phi(x)dx}{\|\phi\|_l}, \tag{2.83}$$

for the numerical solutions. In particular, the computed DG solutions at the final time T are convoluted with a specially chosen kernel, $K_h^{2(r+1),r+1}$, and this will give the post-processed solutions, E_h^* and B_h^*,

$$E_h^* = K_h^{2(r+1),r+1} \star E_h(T,\cdot), \quad B_h^* = K_h^{2(r+1),r+1} \star B_h(T,\cdot). \tag{2.84}$$

The kernel is a linear combination of B-splines functions of order $r+1$, scaled by the mesh size h, and it is translation-invariant. More details can be found in [31] about the kernel. Following essentially the same proof as in [13] (see also [23]), we have the following estimates.

Theorem 2.12. *For the semi-discrete DG method (2.2) (or (2.3)) with the numerical flux (2.5), $\beta_i \geq 0$, $i = 1, 2$, in addition to the L^2-type initialization with $B_h(0,\cdot) = P_h B(0,\cdot)$, $E_h(0,\cdot) = P_h E(0,\cdot)$, if the numerical solutions E_h and B_h are $(r+m)$-th order accurate in L^2 norm and the exact solutions together with the source terms, S_1 and S_2, have sufficient regularity, then the post-processed solutions, E_h^* and B_h^*, will have the following error estimates,*

$$\|E - E_h^*\|, \|B - B_h^*\| \leq Ch^{2r+\min(1,m)}. \tag{2.85}$$

The positive constant C is independent of h. It may depend on r, α, β and some Sobolev norms of the exact solution E and B up to time T.

In both [13] and [23], the analysis is carried out for homogeneous problems. Yet the analysis can be extended directly to the case with smooth source terms, for instance by redefining Θ_M on p.588 in [13] as $\Theta_M = \left(u_0 - P_h u_0, \varphi(0)\right) + \int_0^T (S, \varphi - \chi) dt$, where S is the source term in the problem, also refer to [13] for the notation in this definition.

2.4 Dispersion analysis

In this subsection, we perform dispersion analysis of the proposed general L^2 stable DG methods. The dispersion and dissipation errors of semi-discrete DG methods have been analyzed for scalar linear conservation law [1, 22, 21, 28], and for second-order wave equations [3]. A recent study [2] compares the dispersive behavior of finite element methods, spectral element methods, and DG methods with central flux for the one-way wave equation. As for fully discrete schemes, in [33], Runge-Kutta DG and Lax-Wendroff DG methods are analyzed for linear advection equation. In [27], Runge-Kutta DG methods with the upwind flux are considered for Maxwell's system, and their accuracy in both dispersion and dissipation errors was studied numerically.

In the analysis below, we shall consider the DG scheme (2.2) with flux choice (2.5) and assume $S_1 = S_2 = 0$. As usually done for the dispersion analysis, we use a uniform mesh, i.e. $h_j = h$ for $\forall j$. To carry out the analysis, we assume that the initial condition takes the form

$$E(0, x) = E_0 e^{ikx}, \tag{2.86a}$$

$$B(0, x) = B_0 e^{ikx}, \tag{2.86b}$$

then the exact solution is given by

$$E(t, x) = \frac{E_0 + B_0}{2} e^{i(kx + kt)} + \frac{E_0 - B_0}{2} e^{i(kx - kt)}, \tag{2.87a}$$

$$B(t, x) = \frac{E_0 + B_0}{2} e^{i(kx + kt)} - \frac{E_0 - B_0}{2} e^{i(kx - kt)}. \tag{2.87b}$$

Clearly, it is composed of two waves $e^{i(kx + wt)}$ with the dispersion relation $w = \pm k$.

Now given k, we want to identify the corresponding numerical dispersion relation for the DG methods, where the numerical solution would be composed of waves of the form $e^{i(kx + \tilde{w}t)}$. Below we will discuss the cases of piecewise P^0, P^1, P^2 polynomial spaces, while for higher order polynomials the derivation becomes more cumbersome and is not included in this paper. In all cases, we shall consider the small wavenumber limit, i.e. $kh \to 0$, and perform asymptotic expansion with respect to kh. Compared with [3], our analysis below includes the P^2 polynomial case, and it also provides detailed discussion about both the physical and spurious modes. The specific form of the spurious modes are particularly important to the numerical solutions of non-dissipative (energy-conserving) schemes, i.e. schemes with $\beta_1 = \beta_2 = 0$, verifying their sensitivity to initial data. Same as in error estimates, the parameters α, β_1, β_2 in the numerical flux (2.5) are assumed to be constants of $O(1)$, and $\beta_1 \geq 0$, $\beta_2 \geq 0$.

2.4.1 P^0 polynomials

For the case of piecewise constant polynomial space, we assume $E_h|_{I_j} = E_j$, $B_h|_{I_j} = B_j$. From (2.2), we can obtain the following relation

$$\begin{pmatrix} E_j \\ B_j \end{pmatrix}_t = A_1 \begin{pmatrix} E_{j-1} \\ B_{j-1} \end{pmatrix} + A_2 \begin{pmatrix} E_j \\ B_j \end{pmatrix} + A_3 \begin{pmatrix} E_{j+1} \\ B_{j+1} \end{pmatrix},$$

19

where A_1, A_2, A_3 are 2×2 matrices. From the assumption of the wave taking the form $E_j(t) = \hat{E}(t)e^{ikx_j}$, $B_j(t) = \hat{B}(t)e^{ikx_j}$, the above relation is transformed into

$$\begin{pmatrix} \hat{E} \\ \hat{B} \end{pmatrix}_t = G \begin{pmatrix} \hat{E} \\ \hat{B} \end{pmatrix},$$

where $G = A_1 e^{-ikh} + A_2 + A_3 e^{ikh}$ is the amplification matrix. In particular, G is given by

$$G = \frac{1}{h} \begin{pmatrix} 2\beta_1(\cos(kh) - 1) & 2\alpha(\cos(kh) - 1) + i\sin(kh) \\ -2\alpha(\cos(kh) - 1) + i\sin(kh) & 2\beta_2(\cos(kh) - 1) \end{pmatrix}.$$

The matrix G has two eigenvalues λ_1, λ_2, and we compute

$$\tilde{w}_{1,2} = \frac{\lambda_{1,2}}{i} = \pm k + i\frac{(\beta_1 + \beta_2)k^2}{2}h \pm \frac{\left(-4 + 3(4\alpha^2 - (\beta_1 - \beta_2)^2)\right)k^3}{24}h^2 - i\frac{(\beta_1 + \beta_2)k^4}{24}h^3 + O(k(kh)^4)$$

in the limit of $kh \to 0$. When $\beta_1 + \beta_2 > 0$, this demonstrates a first order dissipation error and in general a second order dispersion error in the numerical solution. If $\beta_1 = \beta_2 = 0$, the scheme is non-dissipative, and the two eigenvalues of G are always real. This can also be verified directly from the analytical form of the amplification matrix G. In this case, the leading dispersion error is of second order unless $\alpha = \pm\sqrt{\frac{1}{3}}$, for which the method can be pushed to have fourth order accuracy in dispersion analysis. This particular parameter choice is also reported in [3].

2.4.2 P^1 polynomials

The procedure is similar for piecewise linear polynomials. By choosing the basis functions on each element I_j to be $\phi_1 = -\xi + \frac{1}{2}$, $\phi_2 = \xi + \frac{1}{2}$, with $\xi = \frac{x - x_j}{h}$, the numerical solution on I_j can be written as $E_h = E_j^1 \phi_1 + E_j^2 \phi_2$, $B_h = B_j^1 \phi_1 + B_j^2 \phi_2$. Similar derivations as in the P^0 case result in the following ODE

$$\begin{pmatrix} \hat{E}^1 \\ \hat{E}^2 \\ \hat{B}^1 \\ \hat{B}^2 \end{pmatrix}_t = G \begin{pmatrix} \hat{E}^1 \\ \hat{E}^2 \\ \hat{B}^1 \\ \hat{B}^2 \end{pmatrix},$$

where the amplification matrix is given by

$$G = \frac{1}{h} \begin{pmatrix} -2\beta_1(2 + e^{ikh}) & \beta_1(2 + 4e^{-ikh}) & 1 - 4\alpha - (1 + 2\alpha)e^{ikh} & 2(1 + \alpha + (-1 + 2\alpha)e^{-ikh}) \\ 2\beta_1(1 + 2e^{ikh}) & \beta_1(-4 - 2e^{-ikh}) & 2(-1 + \alpha + (1 + 2\alpha)e^{ikh}) & -1 - 4\alpha + (1 - 2\alpha)e^{-ikh} \\ 1 + 4\alpha + (-1 + 2\alpha)e^{ikh} & 2(1 - \alpha - (1 + 2\alpha)e^{-ikh}) & -2\beta_2(2 + e^{ikh}) & \beta_2(2 + 4e^{-ikh}) \\ -2(1 + \alpha + (-1 + 2\alpha)e^{ikh}) & -1 + 4\alpha + (1 + 2\alpha)e^{-ikh} & 2\beta_2(1 + 2e^{ikh}) & \beta_2(-4 - 2e^{-ikh}) \end{pmatrix}.$$

The matrix G has four distinct eigenvalues $\lambda_i, i = 1, \ldots, 4$. We perform an asymptotic analysis as $kh \to 0$, and obtain the following results. Four cases are discussed depending on the values of α, β_1, β_2.

Case 1: If $\alpha^2 + \beta_1\beta_2 \neq 0$, then

$$\tilde{w}_{1,2} = \frac{\lambda_{1,2}}{i} = \pm k + i\frac{(\beta_1 + \beta_2)k^4}{288(\alpha^2 + \beta_1\beta_2)}h^3 \mp \frac{k^5}{17280(\alpha^2 + \beta_1\beta_2)^2}(-20\alpha^2 + 96\alpha^4 - 5\beta_1^2 - 5\beta_2^2$$

$$- 30\beta_1\beta_2 + 192\alpha^2\beta_1\beta_2 + 96\beta_1^2\beta_2^2)h^4 + O(k(kh)^5) \tag{2.88a}$$

$$\tilde{w}_{3,4} = \frac{\lambda_{3,4}}{i} = \left(6i(\beta_1 + \beta_2) \pm 6\sqrt{4\alpha^2 - (\beta_1 - \beta_2)^2}\right)\frac{1}{h} + O(1). \tag{2.88b}$$

20

Clearly, $\tilde{w}_{1,2}$ correspond to the physical modes, and $\tilde{w}_{3,4}$ are the spurious modes. If $\beta_1 + \beta_2 > 0$, the leading error in the physical modes is a third order dissipation error. The spurious modes, on the other hand, get damped exponentially fast in time, due to the leading imaginary part of $\tilde{w}_{3,4}$ being positive and proportional to $O(\frac{1}{h})$. If $\beta_1 = \beta_2 = 0$, although the leading error in the physical modes is of higher order, i.e. at least fourth order depending on the value of α, the spurious modes will be $O(\frac{1}{h})$ oscillatory. Therefore, any contribution to the spurious modes from the initial data will always be present over time, rendering the numerical solution highly dependent upon the initial approximation, see Tables 3.3 and 3.4 for numerical verification. We notice that the proposed $\alpha\beta$-fluxes always belong to Case 1.

Case 2: If $\alpha = \beta_1 = 0$, $\beta_2 \neq 0$ then

$$\tilde{w}_{1,2} = \pm k \pm \frac{k^3}{24}h^2 + i\frac{k^4}{72\beta_2}h^3 + O(k(kh)^4), \tag{2.89a}$$

$$\tilde{w}_3 = i\frac{3k^2}{4\beta_2}h + i\frac{k^4}{12\beta_2}\left(\frac{9}{16\beta_2^2} - \frac{3}{4}\right)h^3 + O(k(kh)^4), \tag{2.89b}$$

$$\tilde{w}_4 = i\frac{12\beta_2}{h} + O(1). \tag{2.89c}$$

The leading error in the physical modes $\tilde{w}_{1,2}$ is a second order dispersion error, inferior to Case 1. This shall be held accountable for the sub-optimal order of accuracy illustrated in Table 3.8. For the spurious modes, $\tilde{w}_3$ corresponds to a stationary wave that is not moving with time in the $O(1)$ leading order, but gets damped on the first order of h. $\tilde{w}_4$ on the other hand will be damped exponentially fast due to the leading $O(\frac{1}{h})$ term, and is less significant than $\tilde{w}_3$.

Case 3: If $\alpha = \beta_2 = 0$, $\beta_1 \neq 0$ then

$$\tilde{w}_{1,2} = \pm k \pm \frac{k^3}{24}h^2 + i\frac{k^4}{72\beta_1}h^3 + O(k(kh)^4), \tag{2.90a}$$

$$\tilde{w}_3 = i\frac{3k^2}{4\beta_1}h + i\frac{k^4}{12\beta_1}\left(\frac{9}{16\beta_1^2} - \frac{3}{4}\right)h^3 + O(k(kh)^4), \tag{2.90b}$$

$$\tilde{w}_4 = i\frac{12\beta_1}{h} + O(1). \tag{2.90c}$$

The discussion is similar to Case 2, and is omitted.

Case 4: If $\alpha = \beta_1 = \beta_2 = 0$, then

$$\tilde{w}_{1,2} = \pm\left(k + \frac{k^3}{48}h^2 - \frac{7k^5}{15360}h^4\right) + O(k(kh)^6), \tag{2.91a}$$

$$\tilde{w}_{3,4} = \pm\left(3k - \frac{5k^3}{16}h^2 + \frac{83k^5}{5120}h^4\right) + O(k(kh)^6). \tag{2.91b}$$

In fact, one can show that each $\tilde{w}$ in this case is always real, showing no dissipation error. For the physical modes $\tilde{w}_{1,2}$, the leading error is a second order dispersion error, inferior to Case 1. This shall be held accountable for the suboptimal order of accuracy for the DG methods with the central flux demonstrated numerically in Table 3.7 and predicted in Theorem 2.5. More interestingly, the spurious modes $\tilde{w}_{3,4}$ consists of two waves traveling three times the actual wave speed, and they are not damped with time. The numerical solution, just as in Case 1 with $\beta_1 = \beta_2 = 0$, will be sensitive to the initial approximation.

2.4.3 P^2 polynomials

For the piecewise P^2 polynomial case, we choose the basis functions on each element I_j to be $\phi_1 = 2\xi(\xi - \frac{1}{2})$, $\phi_2 = -4(\xi^2 - \frac{1}{4})$, $\phi_3 = 2\xi(\xi + \frac{1}{2})$ where $\xi = \frac{x - x_j}{h}$. Similar derivations show that there are six eigenvalues of the amplification matrix, and

$$\tilde{w}_{1,2} = \pm k + i\frac{(\beta_1 + \beta_2)k^6}{7200}h^5 \pm \frac{k^7}{252000}(-15 + 56\alpha^2 + 7\beta_1^2 + 7\beta_2^2 + 70\beta_1\beta_2)h^6 + O(k(kh)^7), \tag{2.92a}$$

$$\tilde{w}_{3,4} = \Big(3i(\beta_1 + \beta_2) + 3\sqrt{4\alpha^2 - (\beta_1 - \beta_2)^2}$$
$$\pm \sqrt{6(10 + 6\alpha^2 - 3\beta_1^2 - 3\beta_2^2 + i(3\beta_1 + 3\beta_2)\sqrt{4\alpha^2 - (\beta_1 - \beta_2)^2})}\Big)\frac{1}{h} + O(1), \tag{2.92b}$$

$$\tilde{w}_{5,6} = \Big(3i(\beta_1 + \beta_2) - 3\sqrt{4\alpha^2 - (\beta_1 - \beta_2)^2}$$
$$\pm \sqrt{6(10 + 6\alpha^2 - 3\beta_1^2 - 3\beta_2^2 - i(3\beta_1 + 3\beta_2)\sqrt{4\alpha^2 - (\beta_1 - \beta_2)^2})}\Big)\frac{1}{h} + O(1). \tag{2.92c}$$

$\tilde{w}_{1,2}$ are the physical modes, while $\tilde{w}_{3,4,5,6}$ are the spurious modes. For the physical modes, when $\beta_1 + \beta_2 > 0$, we observe fifth order dissipation error; otherwise, a sixth order dispersion error is dominant. We can verify by basic algebraic manipulations that the imaginary part of the leading term of $\tilde{w}_{3,4,5,6}$ is positive and proportional to $O(\frac{1}{h})$, and this implies that all these spurious modes will decay exponentially with time. We also notice that unlike piecewise linear polynomials, there is no need to distinguish the case of different α, β_1, β_2 values. In fact, we believe this is why the central flux gives sub-optimal accuracy order for the DG methods with piecewise P^1 polynomial spaces, but optimal accuracy order for the P^2 polynomial case in actual simulations.

3 Numerical examples

We perform numerical tests to verify the theoretical results obtained in previous sections, and further demonstrate the behavior of the proposed methods. In particular, we consider

Example 3.1. *Equation (1.1) with $S_1(t, x) = S_2(t, x) = 0$ and the following smooth initial condition*

$$E(0, x) = \sin(x), \quad B(0, x) = -\frac{1}{3}\sin(x).$$

The exact solution is given by

$$E(t, x) = \frac{1}{3}\sin(x + t) + \frac{2}{3}\sin(x - t), \quad B(t, x) = \frac{1}{3}\sin(x + t) - \frac{2}{3}\sin(x - t).$$

Example 3.2. *Equation (1.1) with*

$$S_1(t, x) = \Big(1 - e^{\sin(t)} - \cos(t)\Big)\sin(x), \quad S_2(t, x) = \Big(\sin(t) - \cos(t)e^{\sin(t)}\Big)\cos(x)$$

and zero initial condition $E(0, x) = B(0, x) = 0$.

The exact solution is given by

$$E(t, x) = \sin(t)\sin(x), \quad B(t, x) = (e^{\sin(t)} - 1)\cos(x).$$

In our simulations, we use a ninth-order strong-stability-preserving (SSP) Runge-Kutta method [19] with $\Delta t = O(h)$ for Example 3.1 and a third-order TVD Runge-Kutta method [29] with $\Delta t = O(h^3)$ for Example 3.2 to eliminate the error from the temporal discretization. We remark that the time discretization described in [7] can also be used to solve Example 3.2 without the need to reduce greatly the timestep size in the presence of the source terms.

3.1 Convergence study

We measure the L^2 norm of e_h, L^2 and L^∞ norms of ζ_h, the error in cell averages $e_{ave} = \|\bar{e}_B\| + \|\bar{e}_E\|$, and the L^2 error of the post-processed numerical solution

$$e_h^* = \begin{pmatrix} e_B^* \\ e_E^* \end{pmatrix} := \begin{pmatrix} B \\ E \end{pmatrix} - \begin{pmatrix} B_h^* \\ E_h^* \end{pmatrix}$$

at $t = 15$. The projection Π_h in (2.17) is used to define ζ_h. To compute the L^∞ norm of ζ_h, we sample 20 points in each cell I_j uniformly, and compute the maximum absolute value of ζ_h at all these points. We here examine the superconvergence property of ζ_h in the L^∞ norm as it implies the estimate in (2.52). Unless otherwise noted, the initial condition of the numerical solution is approximated by the L^2 projection. Uniform meshes are used in all numerical tests.

We start with the source free problem, Example 3.1, and first consider the $\alpha\beta$-fluxes with several sets of values for α, β_1, β_2. Tables 3.1, 3.2, 3.3, 3.5, 3.6 list the numerical errors and orders for five sets of the $\alpha\beta$-fluxes. We notice that except for Table 3.3 with flux choice $\alpha = -0.5, \beta_1 = \beta_2 = 0$ (which is also an alternating flux), all other cases demonstrate optimal convergence orders of $r+1, 2r+1, r+2, 2r+1$ for $e_h, e_h^*, \zeta_h, e_{ave}$, respectively. This is in accordance with the theoretical results obtained in Sections 2.2 and 2.3. In particular, the convergence rate for the cell average is higher than the $(r+2)$-th order predicted in Theorem 2.10.

When we restrict our attention to Table 3.3, however, we notice significantly different error behaviors. The convergence orders for e_h, e_h^* still remain $r+1$ and $2r+1$, but the order for ζ_h is reduced to $r+1$ and the order for e_{ave} is oscillating around $r+2$ with mesh refinement. The error terms ζ_h and e_{ave} are also noticeably bigger than their counterparts in Tables 3.1, 3.2, 3.5 and 3.6. We notice that this order reduction does not violate Theorem 2.10, because we have used the L^2 projection to approximate the initial condition instead of the sophisticated initialization prescribed by Lemma 2.9. To verify this claim, we perform a numerical experiment by changing the initial approximation to $\Pi_h(B, E)$ as defined in (2.17), and list the numerical errors and orders in Table 3.4. The projection Π_h is closer to the suggested initial condition in Lemma 2.9 than the L^2 projection, and therefore this results in significantly reduced errors in ζ_h and e_{ave}. In particular, the order of ζ_h is observed to be $r+2$, and the order of e_{ave} is now oscillating about $2r+1$. From these computations, we can draw the conclusion that for this non-dissipative scheme with an $\alpha\beta$ flux where $\beta_1 = \beta_2 = 0$, the superconvergence properties are sensitive to the initialization. This is natural due to the lack of dissipation in the numerical scheme, and is also verified by the dispersion analysis in Section 2.4. When comparing Table 3.3 with Tables 3.5 and 3.6, we observe that dissipation in the numerical schemes can dramatically increase the superconvergence property even if the initial condition is simply approximated by the L^2 projection. The impact of the numerical initialization on superconvergence of DG solutions for one-dimensional linear scalar hyperbolic equations has been previously reported in [34, 6].

We then consider numerical results computed by DG methods with three fluxes that do not belong to the $\alpha\beta$-flux family. In those cases, the operator Π_h does not generate functions closer to the numerical solutions than E, B themselves, so we only list the errors for e_h, e_h^*, e_{ave}. Table

3.7 contains the numerical results for the central flux with $\alpha = \beta_1 = \beta_2 = 0$. We observe sub-optimal r-th order accuracy for odd polynomials P^1 and P^3, and optimal $(r+1)$-th order accuracy for even polynomials P^2 in the L^2 error of the numerical solution. The convergence orders for the post-processed solutions are $2r, 2r + 2, 2r$ respectively for P^1, P^2, P^3. As for the error for cell averages e_{ave}, the convergence orders are all above $r+1$, and seem to oscillate with mesh refinement. Although this flux is energy-conserving similarly to the alternating flux presented in Tables 3.3 and 3.4, the loss of L^2 convergence rate is an indication of the importance of choosing the correct parameters α, β_1, β_2 in the numerical fluxes for the optimal convergence rate.

In Table 3.8, we test the numerical flux with $\alpha = \beta_1 = 0$, $\beta_2 = 0.1$. This is neither an $\alpha\beta$-flux, nor energy-conserving. The errors behave very similarly to the central flux, i.e. only sub-optimal orders are observed for P^1 and P^3 polynomials. On the other hand, Table 3.9 for the numerical flux with $\alpha = 0, \beta_1 = \beta_2 = \sqrt{0.25 - 0.499^2} \approx 0.0316$ shows quite different behavior. By using nonzero values in both β_1 and β_2, this dissipative scheme demonstrates optimal L^2 convergence rate of $(r+1)$-th order for all polynomial cases. Although this flux does not belong to the $\alpha\beta$-fluxes family nor its variant in (2.44), and is not backed up by convergence theory in Section 2.2, we do observe orders of $r + 1, 2r + 1, 2r + 1$ for e_h, e_h^*, e_{ave}, respectively.

Next, we turn our attention to Example 3.2 with the source term. We provide results for numerical errors and orders in Tables 3.10, 3.11, 3.12 for upwind, alternating and central flux. They demonstrate similar behaviors in accuracy orders as their counterparts for the source free problem in Tables 3.1, 3.4, 3.7. We want to emphasize that this example has zero initial condition, and that's why the behavior of the alternating flux in this case is similar to Table 3.4, but not to Table 3.3.

Table 3.1: Example 3.1. Numerical errors and orders at $t = 15$ computed with an $\alpha\beta$-flux, $\alpha = 0$, $\beta_1 = \beta_2 = 0.5$. This is also known as the upwind flux.

space	N	e_h		e_h^*		ζ_h		ζ_h		e_{ave}	
		L^2 error	order	L^2 error	order	L^2 error	order	L^∞ error	order	L^2 error	order
P^1	20	6.53E-03		4.84E-03		4.78E-03		6.22E-03		6.69E-03	
	40	1.30E-03	2.32	6.05E-04	3.00	6.02E-04	2.99	7.70E-04	3.01	8.48E-04	2.98
	80	3.03E-04	2.11	7.55E-05	3.00	7.54E-05	3.00	9.58E-05	3.01	1.06E-04	2.99
	160	7.44E-05	2.03	9.42E-06	3.00	9.43E-06	3.00	1.20E-05	3.00	1.33E-05	3.00
P^2	20	1.24E-04		7.07E-06		6.50E-06		1.10E-05		6.68E-06	
	40	1.56E-05	3.00	1.85E-07	5.25	3.22E-07	4.33	7.67E-07	3.84	2.11E-07	4.99
	80	1.94E-06	3.00	5.22E-09	5.15	1.87E-08	4.11	5.39E-08	3.83	6.60E-09	5.00
	160	2.43E-07	3.00	1.54E-10	5.18	1.15E-09	4.03	3.55E-09	3.92	2.06E-10	5.00
P^3	20	2.52E-06		7.49E-08		6.28E-08		2.45E-07		3.39E-09	
	40	1.57E-07	4.00	3.08E-10	7.92	1.96E-09	5.00	7.67E-09	5.00	2.67E-11	6.99
	80	9.85E-09	4.00	1.31E-12	7.88	6.12E-11	5.00	2.40E-10	5.00	2.09E-13	7.00
	160	6.15E-10	4.00	5.96E-15	7.75	1.91E-12	5.00	7.49E-12	5.00	1.44E-15	7.18

24

Table 3.2: Example 3.1. Numerical errors and orders at $t = 15$ computed with an $\alpha\beta$-flux, $\alpha = 0.4$, $\beta_1 = \beta_2 = 0.3$.

space	N	e_h		e_h^*		ζ_h		ζ_h		e_{ave}	
		L^2 error	order	L^2 error	order	L^2 error	order	L^∞ error	order	L^2 error	order
P^1	20	5.40E-03		2.97E-03		2.91E-03		3.98E-03		4.07E-03	
	40	1.21E-03	2.15	3.67E-04	3.02	3.65E-04	2.99	4.96E-04	3.01	5.12E-04	2.99
	80	2.95E-04	2.04	4.56E-05	3.01	4.56E-05	3.00	6.19E-05	3.00	6.41E-05	3.00
	160	7.33E-05	2.01	5.67E-06	3.01	5.70E-06	3.00	7.74E-06	3.00	8.01E-06	3.00
P^2	20	1.22E-04		5.20E-06		5.02E-06		1.41E-05		4.05E-06	
	40	1.52E-05	3.00	1.26E-07	5.36	2.75E-07	4.19	8.22E-07	4.10	1.27E-07	4.99
	80	1.91E-06	3.00	3.37E-09	5.23	1.65E-08	4.05	4.98E-08	4.05	3.98E-09	5.00
	160	2.39E-07	3.00	9.63E-11	5.13	1.02E-09	4.01	3.07E-09	4.02	1.24E-10	5.00
P^3	20	2.45E-06		7.40E-08		5.29E-08		1.44E-07		2.06E-09	
	40	1.54E-07	4.00	3.01E-10	7.94	1.65E-09	5.00	4.54E-09	4.99	1.62E-11	6.99
	80	9.63E-09	4.00	1.23E-12	7.94	5.16E-11	5.00	1.42E-10	5.00	1.26E-13	7.00
	160	6.02E-10	4.00	5.51E-15	7.80	1.61E-12	5.00	4.45E-12	5.00	7.91E-16	7.32

Table 3.3: Example 3.1. Numerical errors and orders at $t = 15$ computed with an $\alpha\beta$-flux, $\alpha = -0.5$, $\beta_1 = \beta_2 = 0$. This is also known as the alternating flux.

space	N	e_h		e_h^*		ζ_h		ζ_h		e_{ave}	
		L^2 error	order	L^2 error	order	L^2 error	order	L^∞ error	order	L^2 error	order
P^1	20	3.96E-03		2.40E-04		3.48E-03		8.41E-03		3.10E-04	
	40	1.67E-03	1.25	2.74E-05	3.13	8.82E-04	1.98	2.15E-03	1.97	7.49E-05	2.05
	80	2.93E-04	2.51	3.25E-06	3.08	2.20E-04	2.00	5.38E-04	2.00	6.71E-06	3.48
	160	8.94E-05	1.71	4.13E-07	2.98	5.57E-05	1.98	1.36E-04	1.98	9.03E-07	2.89
	320	1.54E-05	2.54	5.10E-08	3.02	1.39E-05	2.01	3.39E-05	2.01	2.42E-08	5.22
P^2	20	1.65E-04		2.38E-06		8.21E-05		2.33E-04		4.81E-06	
	40	1.65E-05	3.32	3.80E-08	5.97	1.01E-05	3.02	3.07E-05	2.92	4.78E-07	3.33
	80	2.07E-06	2.99	6.20E-10	5.94	1.34E-06	2.92	4.00E-06	2.94	4.44E-09	6.75
	160	2.27E-07	3.19	1.11E-11	5.80	1.69E-07	2.99	5.04E-07	2.99	3.17E-10	3.81
P^3	20	2.73E-06		7.25E-08		1.21E-06		3.74E-06		4.65E-08	
	40	1.76E-07	3.96	2.90E-10	7.97	6.75E-08	4.17	1.32E-07	4.83	2.64E-09	4.14
	80	8.52E-09	4.37	1.14E-12	7.99	4.06E-09	4.05	7.96E-09	4.05	8.67E-11	4.93
	160	6.60E-10	3.69	4.82E-15	7.88	2.48E-10	4.03	5.06E-10	3.98	2.52E-12	5.10

Table 3.4: Example 3.1. Numerical errors and orders at $t = 15$ computed with an $\alpha\beta$-flux, $\alpha = -0.5$, $\beta_1 = \beta_2 = 0$ (alternating flux). We use the special projection $\Pi_h(B, E)$ as the initial condition.

space	N	e_h		e_h^*		ζ_h		ζ_h		e_{ave}	
		L^2 error	order	L^2 error	order	L^2 error	order	L^∞ error	order	L^2 error	order
P^1	20	4.41E-03		2.81E-04		2.76E-04		5.48E-04		3.06E-04	
	40	1.11E-03	1.99	3.18E-05	3.15	4.97E-05	2.47	9.76E-05	2.49	3.63E-05	3.08
	80	2.77E-04	2.00	3.85E-06	3.04	4.65E-06	3.42	1.05E-05	3.21	4.24E-06	3.10
	160	6.98E-05	1.99	4.78E-07	3.01	6.53E-07	2.83	1.39E-06	2.92	5.33E-07	2.99
	320	1.74E-05	2.00	5.96E-08	3.00	6.16E-08	3.41	1.37E-07	3.35	6.51E-08	3.03
P^2	20	1.12E-04		2.37E-06		7.85E-06		2.03E-05		6.92E-07	
	40	1.42E-05	2.98	3.82E-08	5.96	2.58E-07	4.92	7.61E-07	4.74	5.27E-09	7.04
	80	1.76E-06	3.01	6.32E-10	5.92	2.63E-08	3.30	8.90E-08	3.10	4.95E-10	3.41
	160	2.21E-07	2.99	1.18E-11	5.75	9.60E-10	4.77	3.27E-09	4.76	5.03E-12	6.62
P^3	20	2.25E-06		7.25E-08		9.19E-08		1.85E-07		3.76E-09	
	40	1.40E-07	4.01	1.14E-12	7.99	3.01E-09	4.93	7.64E-09	4.60	2.36E-11	7.31
	80	8.73E-09	4.00	1.14E-12	7.99	5.58E-11	5.76	2.15E-10	5.15	3.14E-13	6.23
	160	5.46E-10	4.00	4.96E-15	7.84	2.99E-12	4.22	7.52E-12	4.84	5.97E-15	5.72

Table 3.5: Example 3.1. Numerical errors and orders at $t = 15$ computed with an $\alpha\beta$-flux, $\alpha = -0.5$, $\beta_1 = 0$, $\beta_2 = 0.5$.

space	N	e_h		e_h^*		ζ_h		ζ_h		e_{ave}	
		L^2 error	order	L^2 error	order	L^2 error	order	L^∞ error	order	L^2 error	order
P^1	20	5.00E-03		2.57E-03		2.34E-03		3.13E-03		3.31E-03	
	40	1.13E-03	2.14	3.16E-04	3.02	2.93E-04	3.00	3.94E-04	2.99	4.16E-04	2.99
	80	2.75E-04	2.04	3.91E-05	3.01	3.66E-05	3.00	4.94E-05	3.00	5.20E-05	3.00
	160	6.82E-05	2.01	4.86E-06	3.01	4.58E-06	3.00	6.18E-06	3.00	6.50E-06	3.00
P^2	20	1.14E-04		4.79E-06		4.84E-06		1.27E-05		3.45E-06	
	40	1.42E-05	3.01	1.14E-07	5.40	2.77E-07	4.13	7.76E-07	4.03	1.08E-07	4.99
	80	1.77E-06	3.00	2.97E-09	5.26	1.69E-08	4.03	4.79E-08	4.02	3.39E-09	5.00
	160	2.20E-07	3.00	8.35E-11	5.15	1.05E-09	4.01	2.97E-09	4.01	1.06E-10	5.01
P^3	20	2.28E-06		7.37E-08		5.64E-08		1.96E-07		1.66E-09	
	40	1.42E-07	4.01	2.99E-10	7.95	1.76E-09	5.00	6.09E-09	5.01	1.29E-11	7.00
	80	8.84E-09	4.00	1.21E-12	7.95	5.49E-11	5.00	1.90E-10	5.00	1.02E-13	6.99
	160	5.52E-10	4.00	5.41E-15	7.81	1.71E-12	5.00	5.92E-12	5.00	5.96E-16	7.41

Table 3.6: Example 3.1. Numerical errors and orders at $t = 15$ computed with an $\alpha\beta$-flux, $\alpha = -0.499$, $\beta_1 = \beta_2 = \sqrt{0.25 - \alpha^2} \approx 0.0316$.

space	N	e_h		e_h^*		ζ_h		ζ_h		e_{ave}	
		L^2 error	order	L^2 error	order	L^2 error	order	L^∞ error	order	L^2 error	order
P^1	20	4.49E-03		4.72E-04		4.35E-04		7.24E-04		5.77E-04	
	40	1.12E-03	2.01	5.22E-05	3.18	5.34E-05	3.03	8.74E-05	3.05	7.04E-05	3.03
	80	2.79E-04	2.00	6.13E-06	3.09	6.65E-06	3.00	1.08E-05	3.02	8.71E-06	3.02
	160	6.98E-05	2.00	7.43E-07	3.04	8.31E-07	3.00	1.34E-06	3.01	1.08E-06	3.01
P^2	20	1.14E-04		2.67E-06		4.34E-06		1.09E-05		5.18E-07	
	40	1.42E-05	3.00	4.73E-08	5.82	2.73E-07	3.99	6.84E-07	4.00	1.55E-08	5.07
	80	1.78E-06	3.00	9.03E-10	5.71	1.70E-08	4.00	4.26E-08	4.00	4.778E-10	5.02
	160	2.22E-07	3.00	1.94E-11	5.54	1.06E-09	4.00	2.66E-09	4.00	1.48E-11	5.01
P^3	20	2.25E-06		7.27E-08		2.25E-07		5.74E-07		7.37E-09	
	40	1.42E-07	3.98	2.91E-10	7.97	4.45E-09	5.63	7.69E-09	6.22	2.10E-10	5.14
	80	8.79E-09	4.02	1.15E-12	7.99	1.01E-10	5.48	3.36E-10	4.52	1.28E-12	7.35
	160	5.50E-10	4.00	4.89E-15	7.87	1.70E-12	5.90	5.04E-12	6.06	1.75E-15	9.52

Table 3.7: Example 3.1. Numerical errors and orders at $t = 15$ computed with the central flux, $\alpha = \beta_1 = \beta_2 = 0$.

space	N	e_h		e_h^*		e_{ave}	
		L^2 error	order	L^2 error	order	L^2 error	order
P^1	20	3.97E-02		2.29E-02		3.27E-02	
	40	1.75E-02	1.18	5.77E-03	1.99	8.08E-03	2.02
	80	8.43E-03	1.05	1.44E-03	2.00	2.01E-03	2.00
	160	4.18E-03	1.01	3.61E-04	2.00	5.03E-04	2.00
P^2	20	7.91E-05		2.44E-06		2.40E-07	
	40	9.53E-06	3.05	3.86E-08	5.98	1.62E-08	3.89
	80	1.18E-06	3.02	6.05E-10	6.00	1.00E-09	4.02
	160	1.47E-07	3.00	9.62E-12	6.00	4.18E-11	4.58
	320	1.84E-08	3.00	1.48E-13	5.98	1.46E-12	4.84
P^3	20	1.69E-05		7.39E-08		1.03E-08	
	40	1.26E-07	7.07	3.56E-10	7.70	9.38E-10	3.46
	80	6.57E-08	0.94	3.67E-12	6.60	1.46E-10	2.68
	160	1.05E-08	2.64	5.08E-14	6.08	1.56E-12	6.56
	320	1.38E-09	2.93	8.82E-16	5.85	2.08E-13	2.90

Table 3.8: Example 3.1. Numerical errors and orders at $t = 15$ computed with the flux using $\alpha = \beta_1 = 0., \beta_2 = 0.1$.

space	N	e_h		e_h^*		e_{ave}	
		L^2 error	order	L^2 error	order	L^2 error	order
P^1	20	4.30E-02		2.78E-02		3.77E-02	
	40	2.47E-02	0.80	8.58E-03	1.70	1.18E-02	1.68
	80	1.38E-02	0.83	2.52E-03	1.77	3.56E-03	1.72
	160	7.01E-03	0.98	6.75E-04	1.90	9.79E-04	1.86
P^2	20	7.74E-05		2.93E-06		1.04E-06	
	40	9.66E-06	3.00	5.37E-08	5.77	1.62E-08	3.89
	80	1.21E-06	3.00	1.07E-09	5.64	6.73E-10	5.15
	160	1.51E-07	3.00	2.42E-11	5.47	2.52E-11	4.74
	320	1.89E-08	3.00	6.10E-13	5.31	8.86E-13	4.83
P^3	20	1.74E-05		8.13E-08		2.26E-08	
	40	3.37E-06	2.36	5.70E-10	7.16	4.57E-10	5.63
	80	6.83E-07	2.30	8.69E-12	6.04	1.22E-11	5.22
	160	1.15E-07	2.58	1.67E-13	5.70	6.58E-13	4.22
	320	1.53E-08	2.90	3.07E-15	5.76	1.96E-14	5.07

Table 3.9: Example 3.1. Numerical errors and orders at $t = 15$ computed with the flux using $\alpha = 0$, $\beta_1 = \beta_2 = \sqrt{0.25 - 0.499^2} \approx 0.0316$.

space	N	e_h		e_h^*		e_{ave}	
		L^2 error	order	L^2 error	order	L^2 error	order
P^1	20	2.65E-02		2.18E-02		2.97E-02	
	40	8.56E-03	1.63	4.88E-03	2.16	6.33E-03	2.23
	80	2.82E-03	1.60	9.09E-04	2.42	1.16E-03	2.45
	160	8.20E-04	1.78	1.37E-04	2.73	1.85E-04	2.65
	320	2.16E-04	1.92	1.82E-05	2.91	2.54E-05	2.87
	640	5.48E-05	1.98	2.31E-06	2.98	3.26E-06	2.96
P^2	20	7.73E-05		2.74E-06		9.44E-07	
	40	9.58E-06	3.01	4.78E-08	5.84	1.75E-08	5.75
	80	1.19E-06	3.00	8.92E-10	5.74	4.49E-10	5.29
	160	1.49E-07	3.00	1.85E-11	5.59	1.30E-11	5.11
P^3	20	9.08E-06		7.77E-08		1.75E-08	
	40	9.78E-07	3.22	4.12E-10	7.56	2.27E-10	6.27
	80	8.64E-08	3.50	2.88E-12	7.16	2.42E-12	6.55
	160	6.24E-09	3.79	2.16E-14	7.06	2.28E-14	6.73

Table 3.10: Example 3.2. Numerical errors and orders at $t = 15$ computed with an $\alpha\beta$-flux, $\alpha = 0$, $\beta_1 = \beta_2 = 0.5$. This is also known as the upwind flux.

space	N	e_h		e_h^*		ζ_h		ζ_h		e_{ave}	
		L^2 error	order	L^2 error	order	L^2 error	order	L^∞ error	order	L^2 error	order
	20	6.19E-03		3.74E-03		3.45E-03		4.97E-03		3.57E-03	
P^1	40	1.31E-03	2.24	4.68E-04	3.00	4.35E-04	2.99	6.19E-04	3.01	4.70E-04	2.93
	80	3.09E-04	2.09	5.83E-05	3.00	5.45E-05	3.00	7.72E-05	3.01	6.01E-05	2.97
	160	7.58E-05	2.03	7.28E-06	3.00	6.82E-06	3.00	9.63E-06	3.00	7.59E-06	2.99
	20	1.26E-04		5.74E-06		7.71E-06		1.67E-05		3.87E-06	
P^2	40	1.56E-05	3.02	1.45E-07	5.31	4.45E-07	4.11	1.12E-06	3.91	1.24E-07	4.96
	80	1.93E-06	3.01	4.04E-09	5.17	2.72E-08	4.03	7.17E-08	3.96	3.93E-09	4.98
	160	2.41E-07	3.00	1.19E-10	5.09	1.69E-09	4.01	4.54E-09	3.98	1.24E-10	4.99
	20	2.48E-06		9.40E-08		9.28E-08		3.17E-07		2.33E-08	
P^3	40	1.54E-07	4.01	3.48E-10	8.08	2.82E-09	5.04	9.44E-09	5.07	5.69E-11	8.68
	80	9.57E-09	4.01	1.35E-12	8.01	8.82E-11	5.00	2.95E-10	5.00	1.99E-13	8.16
	160	5.97E-10	4.00	5.90E-15	7.84	2.76E-12	5.00	9.21E-12	5.00	1.04E-15	7.58

Table 3.11: Example 3.2. Numerical errors and orders at $t = 15$ computed with an $\alpha\beta$-flux, $\alpha = -0.5$, $\beta_1 = \beta_2 = 0$ (alternating flux).

space	N	e_h		e_h^*		ζ_h		ζ_h		e_{ave}	
		L^2 error	order	L^2 error	order	L^2 error	order	L^∞ error	order	L^2 error	order
	20	6.11E-03		3.72E-03		3.45E-03		4.95E-03		3.62E-03	
P^1	40	1.31E-03	2.22	4.65E-04	3.00	4.33E-04	2.99	6.85E-04	2.85	4.53E-04	3.00
	80	3.12E-04	2.07	5.82E-05	3.00	5.40E-05	3.00	7.80E-05	3.13	5.65E-05	3.00
	160	7.80E-05	2.00	7.27E-06	3.00	6.76E-06	3.00	1.01E-05	2.95	7.07E-06	3.00
	20	1.27E-04		4.44E-06		1.25E-05		3.23E-05		4.73E-06	
P^2	40	1.61E-05	2.98	1.21E-07	5.19	2.94E-07	5.40	6.67E-07	5.60	1.25E-07	5.24
	80	1.99E-06	3.01	3.64E-09	5.06	3.58E-08	3.04	9.41E-08	2.83	4.22E-09	4.89
	160	2.51E-07	2.99	1.13E-10	5.02	8.69E-10	5.36	2.33E-09	5.33	1.15E-10	5.20
	20	2.59E-06		9.25E-08		1.36E-07		2.97E-07		2.59E-08	
P^3	40	1.61E-07	4.00	3.38E-10	8.10	4.56E-09	4.89	1.16E-08	4.68	9.24E-11	8.13
	80	1.01E-08	4.00	1.27E-12	8.05	7.04E-11	6.02	2.13E-10	5.77	9.48E-13	6.61
	160	6.29E-10	4.00	5.32E-15	7.90	4.55E-12	3.95	1.04E-11	4.36	1.60E-14	5.89

Table 3.12: Example 3.2. Numerical errors and orders at $t = 15$ computed with the central flux, $\alpha = \beta_1 = \beta_2 = 0$.

space	N	e_h		e_h^*		e_{ave}	
		L^2 error	order	L^2 error	order	L^2 error	order
	20	5.82E-02		1.90E-02		1.61E-02	
P^1	40	2.71E-02	1.10	4.74E-03	2.00	4.09E-03	1.98
	80	1.33E-02	1.03	1.18E-03	2.00	1.03E-03	1.99
	160	6.61E-03	1.01	2.96E-04	2.00	2.57E-04	2.00
	20	8.12E-05		2.19E-06		5.42E-07	
	40	1.01E-05	3.01	3.45E-08	5.98	8.51E-09	5.99
P^2	80	1.25E-06	3.00	5.41E-10	6.00	1.27E-10	6.07
	160	1.57E-07	3.00	8.46E-12	6.00	2.21E-12	5.85
	20	1.04E-05		9.94E-08		2.50E-08	
	40	1.66E-06	2.65	4.64E-10	7.74	2.76E-10	6.50
P^3	80	2.17E-07	2.93	3.56E-12	7.03	5.27E-12	5.71
	160	2.73E-08	2.99	4.38E-14	6.35	3.37E-14	7.29

3.2 Time history of L^2 error and energy

In this subsection, we study the time history of the L^2 error of the numerical solutions with various α, β_1, β_2 values for the source free problem Example 3.1. Such numerical investigation has been previously performed in [5, 32] for KdV equations and second-order wave equations, and is important for long time wave propagation problems. Without loss of generality, we only consider P^1, P^2 polynomials on a fixed uniform mesh of $N = 40$.

Figure 3.1 plots the simulation results of P^1 polynomials up to $t = 1000$. In particular, the left subfigure shows the time history of L^2 error for three $\alpha\beta$-fluxes. We can see that the flux with $\alpha = 0.5, \beta_1 = \beta_2 = 0$ performs the best. This flux is energy-conserving and has the least amount of numerical dissipation among the three. The L^2 error oscillates around a certain value relating to the initial discretization and does not seem to grow much with time. The other two $\alpha\beta$-fluxes contain numerical dissipation due to the nonzero values of β_1, β_2, and we can see a clear linear growth of the error as a function of time. In the right subfigure, we compare three energy-conserving fluxes with $\beta_1 = \beta_2 = 0$. They all demonstrate linear growth with respect to time. The alternating flux with $\alpha = -0.5, \beta_1 = \beta_2 = 0$ belongs to the $\alpha\beta$-fluxes family and has the smallest error among the three. The central flux, although energy-conserving, produces rather large errors. This is expected due to the sub-optimal order of the DG method with the central flux.
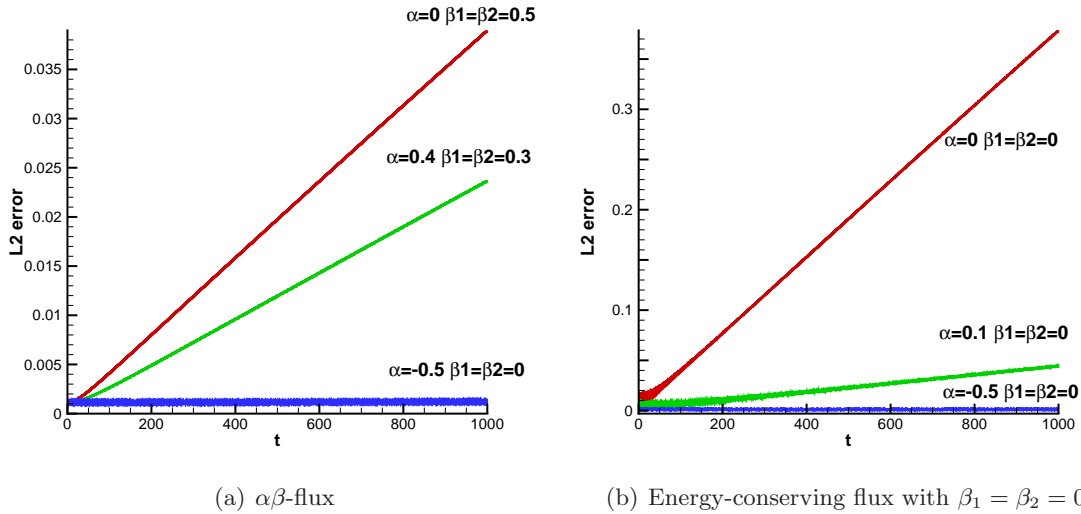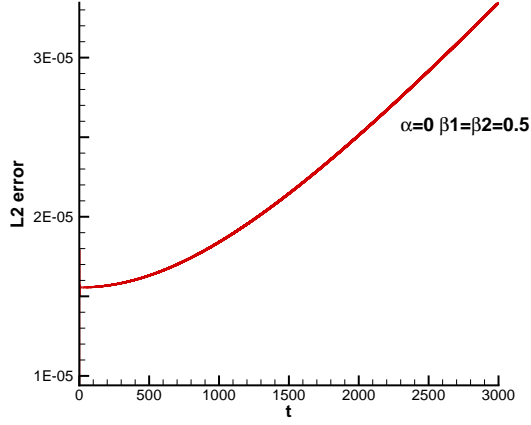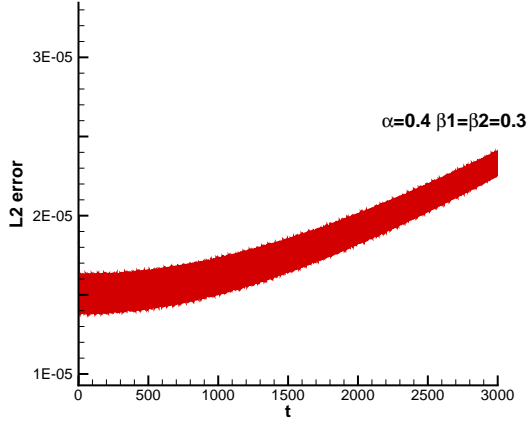

(a) $\alpha\beta$-flux (b) Energy-conserving flux with $\beta_1 = \beta_2 = 0$

Figure 3.1: Example 3.1. Evolution of the L^2 error as a function of time with the indicated fluxes. P^1 polynomials. $N = 40$.

Figure 3.2 plots the simulation results of P^2 polynomials up to $t = 3000$ for four flux choices. They all give comparable numerical errors. The two energy-conserving fluxes with $\beta_1 = \beta_2 = 0$ give the least amount of error growth with respect to time. Compared to Figure 3.1, the error computed with central flux is reduced significantly due to the optimal order of accuracy for P^2 polynomials.
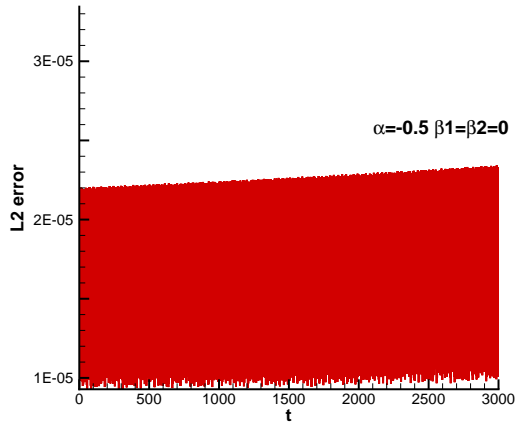
In Figure 3.3, we plot the evolution of the energy as a function of time for three choices of $\alpha\beta$-fluxes. We can see for both P^1 and P^2 polynomials, the energy-conserving flux gives the optimal behavior of conservation as expected from Theorem 2.2.
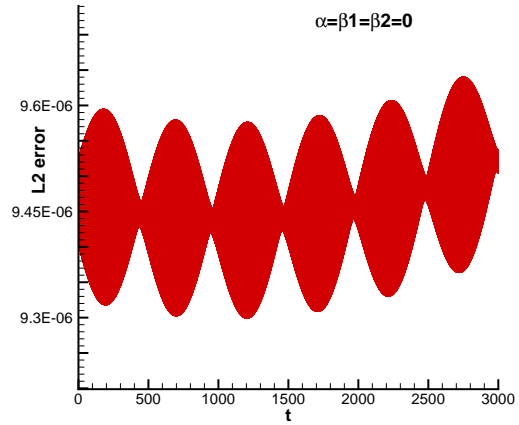
(a) $\alpha = 0.$, $\beta_1 = \beta_2 = 0.5$ (upwind flux)

(b) $\alpha = 0.4$, $\beta_1 = \beta_2 = 0.3$

(c) $\alpha = -0.5$, $\beta_1 = \beta_2 = 0.$ (alternating flux)

(d) $\alpha = 0.$, $\beta_1 = \beta_2 = 0.$ (central flux)

Figure 3.2: Example 3.1. Evolution of the L^2 error as a function of time with the indicated fluxes. P^2 polynomials. $N = 40$.

(a) P^1 polynomials
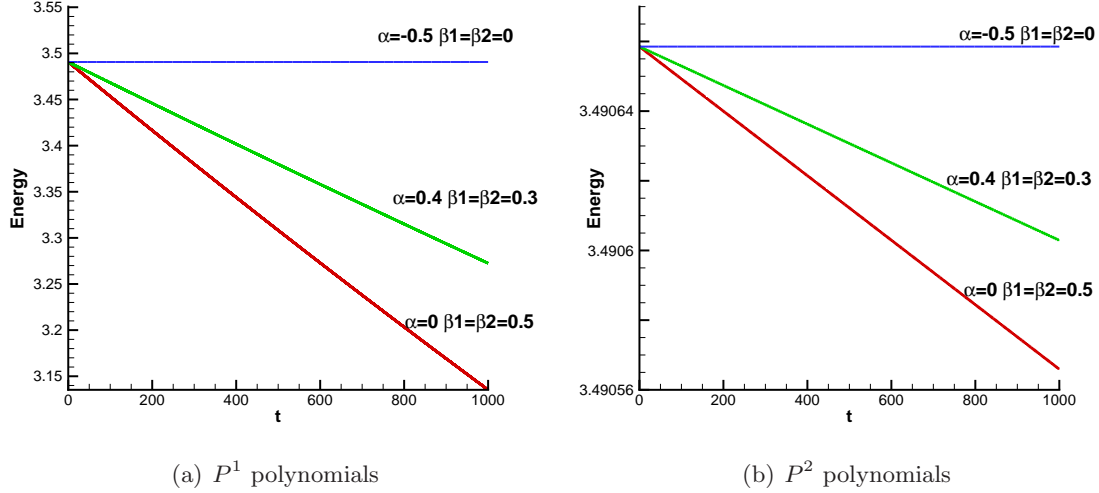

(b) P^2 polynomials

Figure 3.3: Example 3.1. Evolution of the total energy as a function of time with the indicated fluxes. $N = 40$.

4   Conclusion

In this paper, we focus on a general family of L^2 stable high order DG methods for one-dimensional two-way wave equations, as our initial effort to design and analyze accurate and stable methods suitable for long time wave simulation. Theoretical results in terms of stability, accuracy, super-convergence, and dispersion analysis are established systematically.

One novelty of this work is to identify a sub-family of the methods, which have provable optimal L^2 error estimates and superconvergence properties. The analysis relies on a new *local* projection operator. What is more interesting and may be somewhat more challenging is whether some of the new findings around DG methods with provable optimal L^2 accuracy and superconvergence can be extended to higher dimensions. We hope our continuing effort will provide some answers to this in near future. The dispersion analysis in this work also advances our understanding to the numerical performance of some of the proposed methods, and such analysis can be extended to high dimensions, with the algebra expected to be more involved. Note that in [3], dispersion analysis with a different viewpoint was carried out for DG methods with general numerical fluxes (2.5) when the methods are applied to two-dimensional second-order wave equations in their first-order form on tensor product meshes.

A preliminary investigation shows that the L^2 stable numerical fluxes (2.5) with the choice of $\beta_1 = \beta_2 = 0$, and $\alpha \in [-1/2, 0) \cup (0, 1/2]$ also give optimal DG methods for the one dimensional two-way wave equations (1.1), with the use of a *global* projection operator similar to that in [25]. We will leave the detailed study of this case to a future work.

References

[1] M. Ainsworth. Dispersive and dissipative behaviour of high order discontinuous Galerkin finite element methods. *J. Comput. Phys.*, 198(1):106–130, 2004.

[2] M. Ainsworth. Dispersive behaviour of high order finite element schemes for the one-way wave equation. *J. Comput. Phys.*, 259:1–10, 2014.

[3] M. Ainsworth, P. B. Monk, and W. B. Muniz. Dispersive and dissipative properties of discontinuous Galerkin finite element methods for the second-order wave equation. *J. Sci. Comput.*, 27(1-3):5–40, 2006.

[4] M. Ainsworth and H. A. Wajid. Dispersive and dissipative behavior of the spectral element method. *SIAM Journal on Numerical Analysis*, 47(5):3910–3937, 2009.

[5] J. Bona, H. Chen, O. Karakashian, and Y. Xing. Conservative, discontinuous Galerkin methods for the generalized Korteweg-de Vries equation. *Math. Comp.*, 82(283):1401–1432, 2013.

[6] W. Cao, Z. Zhang, and Q. Zou. Superconvergence of discontinuous Galerkin method for linear hyperbolic equations. *arXiv preprint arXiv:1311.6938*, 2013.

[7] M.-H. Chen, B. Cockburn, and F. Reitich. High-order RKDG methods for computational electromagnetics. *Journal of Scientific Computing*, 22(1-3):205–226, 2005.

[8] Y. Cheng and C.-W. Shu. Superconvergence and time evolution of discontinuous Galerkin finite element solutions. *J. Comput. Phys.*, 227(22):9612–9627, 2008.

[9] C.-S. Chou, C.-W. Shu, and Y. Xing. Optimal energy conserving local discontinuous Galerkin methods for second-order wave equation in heterogeneous media. *J. Comput. Phys.*, 272:88–107, 2014.

[10] E. T. Chung and B. Engquist. Optimal discontinuous Galerkin methods for wave propagation. *SIAM J. Numer. Anal.*, 44(5):2131–2158, 2006.

[11] P. G. Ciarlet. *The finite element method for elliptic problems.* North Holland, 1975.

[12] B. Cockburn, S. Y. Lin, and C.-W. Shu. TVB Runge-Kutta local projection discontinuous Galerkin finite element method for conservation laws. III. One-dimensional systems. *J. Comput. Phys.*, 84(1):90–113, 1989.

[13] B. Cockburn, M. Luskin, C.-W. Shu, and E. Süli. Enhanced accuracy by post-processing for finite element methods for hyperbolic equations. *Math. Comp.*, 72(242):577–606, 2003.

[14] B. Cockburn and C.-W. Shu. Runge-Kutta discontinuous Galerkin methods for convection-dominated problems. *J. Sci. Comput.*, 16(3):173–261, 2001.

[15] G. C. Cohen. *Higher-order numerical methods for transient wave equations.* Scientific Computation. Springer-Verlag, Berlin, 2002. With a foreword by R. Glowinski.

[16] L. Fezoui, S. Lanteri, S. Lohrengel, and S. Piperno. Convergence and stability of a discontinuous Galerkin time-domain method for the 3D heterogeneous Maxwell equations on unstructured meshes. *M2AN Math. Model. Numer. Anal.*, 39(6):1149–1176, 2005.

[17] D. Gottlieb and J. S. Hesthaven. Spectral methods for hyperbolic problems. *J. Comput. Appl. Math.*, 128(1-2):83–131, 2001. Numerical analysis 2000, Vol. VII, Partial differential equations.

[18] D. Gottlieb and S. A. Orszag. *Numerical analysis of spectral methods: theory and applications.* Society for Industrial and Applied Mathematics, Philadelphia, Pa., 1977. CBMS-NSF Regional Conference Series in Applied Mathematics, No. 26.

[19] S. Gottlieb, C.-W. Shu, and E. Tadmor. Strong stability-preserving high-order time discretization methods. *SIAM review*, 43(1):89–112, 2001.

[20] M. J. Grote, A. Schneebeli, and D. Schötzau. Discontinuous Galerkin finite element method for the wave equation. *SIAM J. Numer. Anal.*, 44(6):2408–2431, 2006.

[21] F. Hu and H. Atkins. Eigensolution analysis of the discontinuous Galerkin method with nonuniform grids: I. one space dimension. *J. Comput. Phys.*, 182(2):516–545, 2002.

[22] F. Hu, M. Hussaini, and P. Rasetarinera. An analysis of the discontinuous Galerkin method for wave propagation problems. *J. Comput. Phys.*, 151(2):921–946, 1999.

[23] L. Ji, Y. Xu, and J. K. Ryan. Negative-order norm estimates for nonlinear hyperbolic conservation laws. *J. Sci. Comput.*, 54(2-3):531–548, 2013.

[24] R. J. LeVeque. *Finite volume methods for hyperbolic problems.* Cambridge Texts in Applied Mathematics. Cambridge University Press, Cambridge, 2002.

[25] X. Meng, C.-W. Shu, and B. Wu. Optimal error estimates for discontinuous Galerkin methods based on upwind-biased fluxes for linear hyperbolic equations. *Mathematics of Computation*, in press.

[26] W. H. Reed and T. Hill. Triangular mesh methods for the neutron transport equation. *Los Alamos Report LA-UR-73-479*, 1973.

[27] D. Sármány, M. A. Botchev, and J. J. W. van der Vegt. Dispersion and dissipation error in high-order Runge-Kutta discontinuous Galerkin discretisations of the Maxwell equations. *J Sci Comput*, 33(1):47–74, 2007.

[28] S. Sherwin. Dispersion analysis of the continuous and discontinuous Galerkin formulation. *Lect Notes Comp Sci*, 11:425–432, 2000.

[29] C.-W. Shu and S. Osher. Efficient implementation of essentially non-oscillatory shock-capturing schemes. *Journal of Computational Physics*, 77(2):439–471, 1988.

[30] B. Sjögreen and N. A. Petersson. A fourth order accurate finite difference scheme for the elastic wave equation in second order formulation. *J. Sci. Comput.*, 52(1):17–48, 2012.

[31] M. Steffen, S. Curtis, R. M. Kirby, and J. K. Ryan. Investigation of smoothness-increasing accuracy-conserving filters for improving streamline integration through discontinuous fields. *IEEE Trans. Visual. Comput. Graphics*, 14(3):680–692, 2008.

[32] Y. Xing, C.-S. Chou, and C.-W. Shu. Energy conserving local discontinuous Galerkin methods for wave propagation problems. *Inverse Probl. Imag.*, 7(3):967–986, 2013.

[33] H. Yang, F. Li, and J. Qiu. Dispersion and dissipation errors of two fully discrete discontinuous Galerkin methods. *J Sci Comput.*, 55:552–574, 2013.

[34] Y. Yang and C.-W. Shu. Analysis of optimal superconvergence of discontinuous Galerkin method for linear hyperbolic equations. *SIAM J. Numer. Anal.*, 50(6):3110–3133, 2012.

[35] K. Yee. Numerical solution of initial boundary value problems involving Maxwell's equations. *IEEE Trans. Antennas Propag.*, 14(3):302–307, 1966.